Modeling the Syn Disposition of Nitrogen Donors in Non-Heme Diiron Enzymes. Synthesis, Characterization, and Hydrogen Peroxide Reactivity of Diiron(III) Complexes with the Syn N-Donor Ligand H[subscript 2]BPG[subscript 2]DEV

Citation: Friedle, Simone, Jeremy J. Kodanko, Anna J. Morys, Takahiro Hayashi, Pierre Moe#nne-Loccoz, and Stephen J. Lippard. "Modeling the Syn Disposition of Nitrogen Donors in Non-Heme Diiron Enzymes. Synthesis, Characterization, and Hydrogen Peroxide Reactivity of Diiron(III) Complexes with the Syn N-Donor Ligand H2BPG2DEV." Journal of the American Chemical Society 131, no. 40 (October 14, 2009): 14508-14520.

As Published: http://dx.doi.org/10.1021/ja906137y

Publisher: American Chemical Society (ACS)

Persistent URL: http://hdl.handle.net/1721.1/82142

Version: Author's final manuscript: final author's manuscript post peer review, without publisher's formatting or copy editing

Published in final edited form as:
J Am Chem Soc. 2009 October 14; 131(40): 14508–14520. doi:10.1021/ja906137y.

Modeling the Syn-Disposition of Nitrogen Donors in Non-Heme Diiron Enzymes. Synthesis, Characterization, and Hydrogen Peroxide Reactivity of Diiron(III) Complexes with the Syn *N*-Donor Ligand H_2BPG_2DEV

Simone Friedle[†], **Jeremy J. Kodanko**[†], **Anna J. Morys**[†], **Takahiro Hayashi**[‡], **Pierre Moënne-Loccoz**[*,‡], and **Stephen J. Lippard**[*,†]
Department of Chemistry, Massachusetts Institute of Technology, Cambridge, Massachusetts 02139, and Department of Science and Engineering, School of Medicine, Oregon Health & Science University, Beaverton, Oregon 97006-8921

Abstract

In order to model the syn disposition of histidine residues in carboxylate-bridged non-heme diiron enzymes, we prepared a new dinucleating ligand, H_2BPG_2DEV, that provides this geometric feature. The ligand incorporates biologically relevant carboxylate functionalities, which have not been explored as extensively as nitrogen-only analogs. Three novel oxo-bridged diiron(III) complexes $[Fe_2(\mu\text{-}O)(H_2O)_2\text{-}(BPG_2DEV)](ClO_4)_2$ (**6**), $[Fe_2(\mu\text{-}O)(\mu\text{-}O\ CAr^{iPrO})(BPG_2DEV)](ClO_4)$ (**7**), and $[Fe_2(\mu\text{-}O)(\mu\text{-}CO_3)(BPG_2DEV)]$ (**8**) were prepared. Single crystal X-ray structural characterization confirms that two pyridines are bound syn with respect to the Fe–Fe vector in these compounds. The carbonato-bridged complex **8** forms quantitatively from **6** in a rapid reaction with gaseous CO_2 in organic solvents. A common maroon-colored intermediate (λ_{max} = 490 nm; ε = 1500 M_{-1} cm^{-1}) forms in reactions of **6**, **7**, or **8** with H_2O_2 and NEt_3 in CH_3CN/H_2O solutions. Mass spectrometric analyses of this species, formed using ^{18}O-labeled H_2O_2, indicate the presence of a peroxide ligand bound to the oxo-bridged diiron(III) center. The Mössbauer spectrum at 90 K of the EPR-silent intermediate exhibits a quadrupole doublet with δ = 0.58 mm/s and ΔE_Q = 0.58 mm/s. The isomer shift is typical for a peroxodiiron(III) species, but the quadrupole splitting parameter is unusually small compared to related complexes. These Mössbauer parameters are comparable to those observed for a peroxo intermediate formed in the reaction of reduced toluene/*o*-xylene monooxygenase hydroxylase (ToMOH) with dioxygen. Resonance Raman studies reveal an unusually low-energy O–O stretching mode in the peroxo intermediate that is consistent with a short diiron distance. Although peroxodiiron(III) intermediates generated from **6**, **7**, and **8** are poor O-atom transfer catalysts, they display highly efficient catalase activity, with turnover numbers up to 10,000. In contrast to hydrogen peroxide reactions of diiron(III) complexes that lack a dinucleating ligand, the intermediates generated here could be reformed in significant quantities after a second addition of H_2O_2, as observed spectroscopically and by mass spectrometry.

[*]To whom correspondence should be addressed. lippard@mit.eduploccoz@ebs.ogi.edu.
[†]Massachusetts Institute of Technology.
[‡]Oregon Health and Science University.

Supporting Information Available**:** Experimental details for the synthesis of $[^{57}Fe_2(\mu\text{-}O)(H_2O)_2BPG_2DEV](ClO_4)_2$ (^{57}Fe-**6**), crystallographic refinement details, crystallographic tables (Tables S1–S3), a packing diagram of **6** (Fig. S1), ORTEP diagrams of the complete molecules **7** and **8** (Fig. S2 and S3), space-filling diagrams of **6–8** (Fig. S4), and CIF files for **6–8**, UV-vis spectra of **6a** and **7a** (Fig. S5–S7), solution Mössbauer spectra of **7a**, **8a**, **6** and the decomposition product of **6a** (Fig. S8–S11); the EPR spectrum of **8a** (Fig. S12), high-resolution mass spectra of **6a–8a** (Fig.S13 and S14), and a table for substrate oxidation studies (Table S4) are provided. This material is available free of charge via the Internet at http://pubs.acs.org.

Introduction

Carboxylate-bridged non-heme diiron centers occur in a variety of enzymes that activate dioxygen to catalyze key reactions in nature.1–5 Members of this class include ribonucleotide reductase (RNR-R2),6–8 Δ^9-desaturase (Δ^9D),9,10 and the hydroxylase components of bacterial multicomponent monooxygenases (BMMs).11,12 Soluble methane monooxygenase (sMMOH),4 toluene/*o*-xylene monooxygenase (ToMOH),13,14 and phenol hydroxylase (PHH)15 belong to the family of BMMs and function as catalysts for the selective oxidation of hydrocarbons. Remarkably, despite their diverse roles in biology, the active sites in these enzymes all share common structural features, a carboxylate-rich environment with two histidine donors that are bound in a syn fashion with respect to the diiron vector.16 Representations of the active sites of some of these enzymes in their reduced diiron(II) forms are provided in Chart 1.

In these enzymes, dioxygen activation occurs following 2-electron reduction of their diiron(III) resting states to generate an O_2-reactive diiron(II) species. Following reaction of this reduced form with dioxygen, peroxodiiron(III) intermediate species are generated that share common spectroscopic features.4 Resonance Raman spectral studies of peroxo intermediates in RNR-R217 and Δ^9D[10] suggest a μ-1,2-peroxo binding mode. Theoretical analysis of the peroxo intermediate in sMMOH, for which no vibrational spectroscopic data are yet available, find a μ-η^2:η^2-peroxo butterfly structure to be more stable,18 and pH-dependent studies of the dioxygen activation chemistry indicate that proton transfer reactions,19 most likely involving some kind of hydroperoxo intermediate, are involved. Recently, novel peroxodiiron(III) transient intermediates were observed in the ToMOH and PHH systems, having no visible or near-IR optical bands, notably different Mössbauer parameters, and possibly a different coordination mode.12,20 Peroxodiiron(III) intermediates in these enzymes can in some cases undergo O–O bond cleavage to form high-valent species, such as the mixed-valent (μ-oxo)diiron(III,IV) intermediate X in RNR-R26 and the methane-oxidizing di(μ-oxo)diiron(IV) intermediate Q in sMMO.21,22 Elucidating the structures of these oxygenated intermediates remains an important challenge.

Significant effort has been expended to construct model complexes that mimic the active site structures and functions of non-heme diiron enzymes.23,24 These studies have predominantly been conducted to probe the mechanism of O_2 activation, the influence of structure on reactivity, and the requirements of iron-based catalysts for hydrocarbon oxidation. Two general ligand motifs have been extensively employed in the construction of these model complexes, namely, tris(2-pyridylmethyl)amine (TPA)-based and sterically encumbering 2,6-diarylbenzoate ligands (Chart 2).23–26 Whereas the latter group of ligands facilitates formation of diiron(II) complexes with the same composition as the enzyme active sites, TPA-based constructs afford complexes that react with dioxygen to generate species more closely resembling intermediates observed spectroscopically in the reactions of BMMs with dioxygen. A structural feature that neither of these ligand motifs can rigidly enforce, however, is the syn orientation of nitrogen donors with respect to the diiron vector. This feature may be important and it is likely that nature did not choose such a stereochemistry arbitrarily. The significance of the syn *N*-donor disposition of imidazoles from histidine residues with respect to the diiron vector is still unclear, although preliminary DFT calculations on intermediate Q of sMMOH suggest that a stereoelectronic effect derived from this configuration tunes its reactivity.27 Apart from their inability to enforce syn *N*-donor character, terphenylcarboxylate- and TPA-based ligands are not pre-organized to stabilize a diiron core, which can lead to dissociation or aggregation to form monomeric or oligomeric species, respectively. To address these issues, we have been exploring *N*-donor ligands that are covalently tethered by a diethynylbenzene unit.16,28–31 Selection of this moiety as the appropriate linker fixes the nitrogen donor atoms at a distance and

orientation similar to that in the enzymes. Of particular interest is the 1,2-bis(pyridin-3-ylethynyl)benzene scaffold, because of convenience in functionalizing the pyridine moiety, as demonstrated in the synthesis of several ligands based on this platform.28

In the present article we report the synthesis of the syn *N*-donor ligand H_2BPG_2DEV (Chart 2) and three of its derivatives containing oxo-bridged diiron(III) cores. Two tripodal *N,N*-bis(2-pyridylmethyl)-3-aminoacetate (BPG^-) centers bridged by diethynylveratrole converge to incorporate diiron units and provide carboxylate groups that more accurately represent the aspartate and glutamate residues of non-heme diiron enzymes than earlier constructs. We describe how this dinucleating ligand stabilizes the oxo-bridged diiron(III) cores and considerably influences the chemical and physical properties of a peroxodiiron(III) intermediate generated by addition of hydrogen peroxide.

Experimental Section

Materials and Methods

Reagents were purchased from commercial sources and used as received. Acetonitrile (CH_3CN), dichloromethane (CH_2Cl_2), and tetrahydrofuran (THF) were saturated with nitrogen and purified by passing though activated alumina columns under argon. Triethylamine (Et_3N) was distilled from CaH_2. The compounds (5-bromo-pyridin-2-yl)methanol (**2b**),32 [(pyridin-2-ylmethyl)amino]acetic acid ethyl ester (**3**),33 4,5-diethynylveratrole (DEV),31 and $(Et_4N)_2[Fe_2(\mu\text{-}O)Cl_6]$34,35 were prepared using methods described in the literature. The compound 2,6-diisopropoxybenzoic acid (HO_2CAr^{iPrO}) was synthesized by using a modified literature procedure.36 **Caution!** The perchlorate salts used in this study are potentially explosive and should be handled with care!

NMR spectra were recorded on a Varian 300 spectrometer in the Massachusetts Institute of Technology Department of Chemistry Instrument Facility (MIT DCIF). All spectra were recorded at ambient probe temperature, 293 K. IR spectra were taken on a Thermo Nicolet Avatar 360 spectrometer with OMNIC software. Mass spectra were recorded in electrospray ionization mode. ESI-MS data were obtained with an Agilent 1100 series LC/MSD mass spectrometer. UV-vis experiments were performed on a Cary 50 spectrophotometer.

[(5-Bromo-pyridin-2-ylmethyl)-pyridin-2-ylmethyl-amino]acetic Acid Ethyl Ester (4)

A solution of (5-bromo-pyridin-2-yl)methanol (**2b**) (4.69 g, 24.9 mmol) and Et_3N (4.53 mL, 32.4 mmol) in THF (95 mL) was cooled to 0 °C and treated dropwise with methanesulfonyl chloride (MsCl; 2.32 mL, 29.9 mmol). The mixture was warmed to room temperature, stirred for 2 h, and then combined with aqueous NH_4Cl (200 mL). The aqueous phase was extracted with CH_2Cl_2 (3 × 200 mL) and the organic layers were dried (Na_2SO_4), filtered, and concentrated to afford a solid (6.78 g, quant) that was used without further purification. This purple solid, K_2CO_3 (4.12 mg, 29.9 mmol), and [(pyridin-2-ylmethyl)-amino]-acetic acid ethyl ester (**3**) (5.80 g, 29.9 mmol) were stirred overnight in CH_3CN (100 mL). During this period the color changed from purple-red to orange. The reaction mixture was combined with CH_2Cl_2 (300 mL) and the organics were washed with aq Na_2CO_3 (3 × 100 mL). The organic layer was dried (Na_2SO_4), filtered, and evaporated to dryness. The crude product was purified by column chromatography (alumina; EtOAc/hexanes, 1:3) to give **4** as a yellow oil, which was identical to the compound synthesized previously as judged by ^1H NMR spectroscopy and ESI-MS.28 Yield: 7.92 g (87%). ^1H NMR (300 MHz, $CDCl_3$): δ = 8.56–8.50 (m, 2H), 7.67–7.61 (dt, J = 1.8, 7.5 Hz, 1H), 7.29 (d, J = 8.1 Hz, 1H), 7.17–7.12 (m, 2H), 4.19–4.11 (q, J = 7.2 Hz, 2H), 3.96 (s, 2H), 3.94 (s, 2H), 3.44 (s, 2H), 1.27–1.22 (t, J = 7.2 Hz, 3H). LRMS (ESI) calcd for $C_{16}H_{18}BrN_3O_2Na$ $[M+Na]^+$: 386, found: 386.

$Et_2BPG_2DEV{\cdot}2HCl$ (5·2HCl) (Diethyl 2,2'-(5,5'-(4,5-dimethoxy-1,2-phenylene) bis(ethyne-2,1-diyl)bis(pyridine-5,2-diyl))bis(methylene)bis((pyridin-2-ylmethyl)-azane-diyl)diacetate) Hydrochloride

4,5-Diethynylveratrole (0.474 g, 2.55 mmol), **4** (1.82 g, 5.03 mmol), $[Pd(PPh_3)_4]$ (0.250 g, 0.216 mmol), Et_3N (3.6 mL, 26 mmol), and THF (24 mL) were combined in a sealed tube under an inert atmosphere and stirred for 2.5 d at 60 °C. After the reaction mixture was cooled to room temperature, it was combined with EtOAc (50 mL) and washed three times with a solution of Na_2CO_3 (aq.), dried over Na_2SO_4, filtered, and evaporated to dryness. The crude material was purified by column chromatography (alumina; EtOAc/hexanes, 1:1–1:0) to give **5** as thick yellow oil. ^1H NMR spectroscopy confirmed complete conversion to the desired product, but a phosphine oxide impurity was observed. To purify the material, the hydrochloride salt of the amine, **5**·2HCl, was synthesized. The oil was dissolved in ca. 100 mL of EtOAc and ca. 4 mL of a solution of HCl in Et_2O (2 M) was added dropwise with stirring until no further precipitation occurred. The yellow solid was filtered off and dried in vacuum. Yield: 1.20 g (57%). ^1H NMR (300 MHz, CD_3OD): δ = 8.92 (m, 2H); 8.89 (m, 2H); 8.54 (dt, J = 1.5; 7.8 Hz, 2H); 8.37 (dd, J = 2.1, 9.0 Hz, 2H); 8.07 (d, J = 7.8 Hz, 2H); 8.00–7.96 (m, 2H); 7.90 (d, J = 8.4 Hz, 2H); 7.25 (s, 2H); 4.58 (s, 4H); 4.56 (s, 4H); 4.18 (q, J = 7.2 Hz, 4H); 3.92 (s, 6H); 3.74 (s, 4H); 1.25 (t, J = 7.2 Hz, 6H). ^{13}C NMR (125 MHz, CD_3OD): δ = 171.27, 154.21, 153.90, 151.40, 147.44, 146.96, 145.77, 142.35, 127.61, 127.31, 126.77, 122.78, 117.88, 115.47, 94.90, 86.30, 61.68, 56.97, 56.48, 56.24, 54.90, 13.87. HRMS (ESI) calcd for $[M+H]^+$: 753.3397, found: 753.3397. IR (KBr, cm^{-1}): 2979 (m), 2914 (m), 2611 (m), 2214 (m, $\nu_{C\equiv C}$), 1731 (s), 1614 (m), 1593 (m), 1511 (s), 1464 (m), 1371 (m), 1251 (s), 1215 (s), 1155 (m), 1086 (m), 1024 (m), 987 (m), 858 (w), 772 (w). Mp: 103–105 °C.

H_2BPG_2DEV (5a), 2,2'-(5,5'-(4,5-Dimethoxy-1,2-phenylene)bis(ethyne-2,1-diyl)bis(pyridine-5,2-diyl))bis(methylene)bis((pyridin-2-ylmethyl)azanediyl)diacetic Acid

An aqueous solution of **5**·2HCl (0.55 g, 0.67 mmol) and KOH (1.4 g, 25 mmol) were combined to yield a total volume of 100 mL. The resulting suspension was heated to 60 °C under a nitrogen atmosphere for ca. 4 h. After cooling down to room temperature, the reaction mixture was acidified with dilute HCl to pH 5 and the product was extracted with CH_2Cl_2. The organic phase was dried over Na_2SO_4, filtered, and reduced to dryness to yield a yellow-brown solid. Yield: 0.42 g (91%). ^1H NMR (300 MHz, $CDCl_3$): δ = 13.11 (s, 2H), 8.68 (m, 2H), 8.58 (m, 2H), 7.73 (m, 4H), 7.35 (m, 4H), 7.24 (m, 2H), 7.03 (s, 2H), 4.13 (s, 4H), 4.07 (s, 4H), 3.94 (s, 6H), 3.57 (s, 4H). ^{13}C NMR (125 MHz, d_6-DMSO): δ = 173.44, 160.29, 160.05, 151.76, 150.64, 149.93, 139.86, 137.83, 123.93, 123.65, 123.40, 118.94, 118.40, 115.49, 92.16, 90.19, 60.32, 60.22, 57.00, 55.46. HRMS (ESI) calcd for $[M+H]^+$: 697.2770, found: 697.2770. IR (KBr, cm^{-1}): 3054 (w), 3002 (w), 2912 (w), 2832 (w), 2206 (w, $\nu_{C\equiv C}$), 1714 (m), 1637 (w), 1593 (m), 1551 (w), 1511 (s), 1437 (m), 1401 (m), 1359 (m), 1248 (s), 1215 (s), 1149 (m), 1119 (m), 1085 (m), 1024 (m), 993 (m), 858 (w), 761 (m), 722 (m), 695 (m), 649 (w), 621 (w), 541 (m). Mp: 60–62 °C.

$[Fe_2(\mu\text{-}O)(H_2O)_2BPG_2DEV](ClO_4)_2$ (6)

To a solution (2 mL; CH_3CN/H_2O, 10:1) of $Fe(ClO_4)_3{\cdot}9H_2O$ (77 mg, 150 μmol) was added a suspension of **5a** (50 mg, 72 μmol) in the same solvent mixture (2 mL). The color instantly changed to deep-red and the resulting solution was stirred for ca. 5 min. After filtration, the solution was subjected to vapor diffusion of Et_2O to yield crystalline red plates that were analyzed by X-ray crystallography. The yield of crystalline material was highly dependent on the H_2O content of the solution. Yield: 60 mg (78%). X-ray diffraction quality crystals were grown from vapor diffusion of Et_2O into a solution of **6** in CH_3OH and H_2O. LRMS (ESI) calcd for $[M-H]^+$: 857.1, found: 875.2. IR (KBr, cm^{-1}): 3430 (m), 3073(w),

2921 (w), 2854 (w), 2210 (w, $\nu_{C\equiv C}$), 1608 (s), 1590 (s), 1550 (m), 1512 (s), 1492 (m), 1462 (w), 1446 (m), 1402 (w), 1367 (m), 1348 (m), 1301 (w), 1286 (w), 1250 (s), 1212 (m), 1099 (vs), 1086 (vs), 1024 (m), 992 (w), 927 (w), 902 (w), 807 (m, $\nu_{Fe-O-Fe}$), 768 (m), 731 (w), 667 (w), 651 (w), 622 (m), 570 (w), 476 (w), 423 (w). Anal. Calcd. for **6**·2CH_3OH, $C_{42}H_{46}N_6O_{19}Cl_2Fe_2$: C, 44.98; H, 4.13; N, 7.49. Found: C, 45.18; H, 4.19; N, 7.12. UV–vis (CH_3CN:H_2O, 10:1) (λ_{max}, nm (ε, M^{-1} cm^{-1})): 480 (440). Mp: 175–180 °C (dec).

[Fe_2(μ-O)(μ-O_2CAr^{iPrO})BPG_2DEV](ClO_4) (7)

Method A. A red CH_3OH/CH_2Cl_2 (1:1) solution of **6** (63 mg, 60 μmol) was allowed to react with HO_2CAr^{iPrO} (21 mg, 90 μmol) in the presence of NEt_3 (40 μL) to form an intense green solution. Clusters of green needles were isolated by vapor diffusion of Et_2O into this reaction mixture. Yield: 40 mg (57%). **Method B.** A CH_3OH/CH_2Cl_2 (1:1) solution of $Fe(ClO_4)_3$·$9H_2O$ (77 mg, 150 μmol) was combined with HO_2CAr^{iPrO} (19 mg, 79 μmol) and NEt_3 (60 μL). To this reaction mixture, a solution of **5a** (50 mg, 72 μmol) was instantly added and the resulting deep green solution was stirred for 10 min, filtered, and subjected to vapor diffusion of Et_2O. Deep green needle-shaped crystals, suitable for X-ray crystallographic analysis, were isolated. Yield: 38 mg (46%). LRMS (ESI) calcd for [M–ClO_4]$^+$: 1059.2, found: 1059.5. IR (KBr, cm^{-1}): 3076 (w), 2975 (w), 2930 (w), 2211 (w, $\nu_{C\equiv C}$), 1645 (s), 1608 (s), 1593 (s), 1530 (s), 1513 (s), 1459 (s), 1422 (s), 1372 (m), 1356 (m), 1332 (m), 1289 (m), 1249 (s), 1087 (vs), 1024 (m), 996 (w), 923 (w), 906 (w), 848 (w), 834 (w), 771 (m, $\nu_{Fe-O-Fe}$), 729 (w), 668 (w), 623 (m), 551 (w), 512 (w). Anal. Calcd for **7**·0.5CH_2Cl_2, $C_{53.5}H_{53}N_6O_{15}Cl_2Fe_2$: C, 53.43; H, 4.44; N, 6.99. Found: C, 53.84; H, 4.87; N, 7.08. UV–vis ($CHCl_3$:CH_3OH, 1:1) (λ_{max}, nm (ε, M^{-1} cm^{-1})): 642 (130); 522 (sh, 218); 490 (730); 475 (sh, 569); 436 (sh, 1171); 413 (1577). Mp: 195–200 °C (dec).

[Fe_2(μ-O)(μ-CO_3)BPG_2DEV] (8)

A solution (6 mL, CH_2Cl_2/CH_3OH, 1:1) of **5a** (100 mg, 144 μmol) and Et_3N (40 mL, 290 μmol) was added dropwise to a solution (7 mL, CH_2Cl_2/CH_3OH, 1:1) of $(Et_4N)_2$[Fe_2(μ-O)Cl_6] (87 mg, 144 μmol). Solid Ag_2CO_3 (159 mg, 576 μmol) was then added to the brown solution. The resulting suspension turned green and was allowed to react for ca. 45 min. The mixture was filtered and subjected to vapor diffusion of Et_2O. After 2–3 days, emerald-green needles of **8** were harvested that were suitable for X-ray crystallography. Yield: 93 mg (73%). LRMS (ESMS) calcd for $(M+H)^+$: 883.1, found: 883.0; calcd for $(M–CO_3+OH)^+$: 839.1, found: 839.2. IR (KBr, cm^{-1}): 3065 (w), 2956 (w), 2920 (w), 2846 (w), 2210 (w, $\nu_{C\equiv C}$), 1617 (s), 1610 (s), 1571 (w), 1533 (m), 1513 (s), 1495 (m), 1444 (m), 1403 (w), 1383 (w), 1358 (m), 1321 (m), 1304 (m), 1289 (m), 1272 (w), 1248 (m), 1214 (m), 1182 (m), 1158 (w), 1142 (w), 1123 (w), 1102 (w), 1087 (w), 1055 (w), 1040 (w), 1024 (w), 997 (w), 927 (w), 908 (w), 860 (w), 847 (w), 838 (w), 770 (m, $\nu_{Fe-O-Fe}$), 742 (w), 695 (w), 663 (w), 564 (w), 552 (w), 528 (w), 460 (w), 437 (w), 423 (w). UV–vis ($CHCl_3$:CH_3OH, 1:1) (λ_{max}, nm (ε, M^{-1} cm^{-1})): 638 (124); 517 (193); 487 (567); 473 (sh, 342); 411 (1576). Anal. Calcd for **8**·0.75CH_2Cl_2, $C_{41.75H}H_{35.5}N_6O_{10}Cl_{1.5}Fe_2$: C, 53.00; H, 3.78; N, 8.88. Found: C, 52.99; H, 4.27; N, 9.10. Mp: 150–155 °C (dec).

X-ray Crystallographic Studies

Intensity data were collected on a Bruker SMART APEX CCD diffractometer with graphite-monochromated Mo Kα radiation (λ = 0.71073 Å), controlled by a Pentium-based PC running the SMART software package.37 Single crystals were mounted on the tips of glass fibers, coated with Paratone-N oil, and cooled to 110 K under a stream of N_2 maintained by a KRYO-FLEX low-temperature apparatus. A total of 2800 frames were collected for each compound. The structures were solved by direct methods and refined on F^2 by using the SHELXTL-97 software included in the SHELXTL software package.38,39 Empirical

absorption corrections were applied by using the SADABS program,40 and the structures were checked for higher symmetry with the PLATON software.41 All non-hydrogen atoms were located and their positions refined with anisotropic thermal parameters by least-squares cycles. All hydrogen atoms were assigned to idealized positions and given thermal parameters equivalent to either 1.5 (methyl hydrogen atoms) or 1.2 (all other hydrogen atoms) times the thermal parameter of the carbon atoms to which they were attached. The hydrogen atoms of O8 and O9 of the H_2O ligands in the diiron(III) complex **6** and of O1W were located from a difference map and their bond distances to the corresponding oxygen atoms restrained using a DFIX command. Refinement details, data collection parameters, and crystal data for **6**, **7**, and **8** are reported in the Supporting Information.

Mössbauer Spectroscopy

Mössbauer spectra were recorded on an MSI spectrometer (WEB Research Company) with a ^{57}Co source in a Rh matrix maintained at room temperature. Solid samples of **6**, **7**, and **8** were prepared by suspension of 13 to 20 mg of the powdered solids in Apiezon M grease and placed in a nylon sample holder. Solution samples of reaction intermediates **8a** and **7a** were prepared by respectively treating suspensions (ca. 0.8 mL) of the oxo-bridged diiron complexes **8** (ca. 20 μmol, CH_3CN/H_2O, 1:1) and **7** (ca. 10 μmol, CH_3OH/H_2O, 4:1) with Et_3N (15 μL) followed by addition of aqueous solution of H_2O_2 (50 μL, 30%). After ca. 1 min, the red-brown reaction mixture was transferred to a sample holder and instantly frozen in liquid N_2. A sample of **6a** was prepared similarly, but using a more dilute solution (ca. 2 μmol, CH_3OH/H_2O, 20:1) of ^{57}Fe-enriched complex **6**, ^{57}**Fe-6**, which was allowed to react with Et_3N (5 μL) and excess H_2O_2 (10 μL, 30%) for ca. 40–50 s and then frozen instantly. The synthesis of ^{57}**Fe-6** is described in Supporting Information. Data were acquired at 4.2 K and 90 K, and isomer shift (δ) values are reported relative to the room temperature Mössbauer spectrum of a metallic iron foil, which was used for calibration of the velocity scale. The spectra were fit to Lorentzian lines with the WMOSS plot and fit program.42

Resonance Raman Spectroscopy

Resonance Raman (RR) spectra were obtained on a custom built McPherson 2061/207 spectrometer equipped with a Princeton Instrument liquid-N_2 cooled CCD detector (LN-1100PB). Excitation at 647, 568, and 413 nm was provided by a Kr laser (Innova 302, Coherent) and 514- and 488- nm excitations by an Ar laser (Innova 90, Coherent). The laser beam was kept at low power, between 40 and 10 mW, and was focused with a cylindrical lens onto frozen samples in NMR tubes. Long wave pass filters (RazorEdge filters, Semrock) or super-notch filters (Kaiser Inc.) were used to attenuate Rayleigh scattering. Sets of ~4 min accumulations were acquired at 4-cm^{-1} resolution. Frequency calibrations were performed using aspirin and are accurate to ±1 cm^{-1}. The samples were subjected to continuous spinning at 110 K to prevent adverse effects from laser illumination. Regular visual inspection of the sample colors during the course of the RR experiments and comparison of consecutive RR spectra provided a reliable means to evaluate photobleaching of species of interest.

Electrospray Ionization Mass Spectrometry of the Peroxo Intermediate

Products **6a**, **7a**, and **8a**, which result from reaction of H_2O_2 and NEt_3 with **6**, **7**, or **8**, respectively, were identified by ESI-MS using a Finnigan LTQ ion trap mass spectrometer maintained at the Department of Chemistry, Tufts University. The samples were prepared by addition of a 50–100 fold excess of a 2% aqueous H_2O_2 solution containing 5 equiv of NEt_3 to solutions of the diiron(III) complexes (ca. 1–2 mM) in solvent mixtures of CH_3CN/H_2O or CH_3OH/CH_2Cl_2. The peaks of interest were confirmed by comparison of the observed and calculated *m/z* values including isotope patterns.

Reaction of 6, 7, and 8 with H_2O_2 and Quantification of O_2 Evolution

In order to quantify the amount of dioxygen formed during hydrogen peroxide decomposition, 2 mL of a 0.4 mM solution of the diiron complex were placed in a 25-mL round-bottom flask equipped with a stir bar. The flask was then tightly sealed with a rubber septum and electrical tape. The solution was treated with ca. 5 μL of NEt_3 and cooled to 0 °C before H_2O_2 was added through the septum with a syringe. The concentration of diiron complex was kept constant by adjusting the final volume of the reaction mixture. The reaction flask was connected by a cannula to an inverted graduated cylinder, filled with H_2O, and the amount of O_2 generated was determined applying the ideal gas law. In the case of **6**, the solution was thoroughly purged with nitrogen to remove any traces of CO_2 that can potentially react with **6** under basic conditions to form the carbonato-bridged complex **8**.

Substrate Oxidation Studies

Oxidation reactions were carried out under an inert atmosphere of N_2 (g). In each experiment, *cis*-cyclooctene (0.26 mL, 2.0 mmol) and NEt_3 (5 μL) were added to 2.0 mL of a 1.0 M solution of **6** or **7** in CH_3CN/H_2O (95:5) at 25 °C. To this mixture, H_2O_2 (97 μL, 10.3 M; diluted with CH_3CN to a total volume of 400 μL) was added by syringe pump over a period of one h. After stirring for an additional 2h, the products were determined by GC analysis. The structures of the products were confirmed by GC-MS spectrometry, and by comparison with authentic samples.

Results and Discussion

Synthesis of H_2BPG_2DEV (5a)

Previously we reported an efficient route to a new family of diethynyltriptycene-linked dipyridyl ligands, including Et_2BPG_2DET (DET = 2,3-diethynyltriptycene), an analog of Et_2BPG_2DEV (**5**).28 Our initial route started from commercially available 2,5-dibromopyridine (**1**). Following a known reaction, we synthesized 2-formyl-5-bromopyridine (**2a**) by treatment of **1** with *n*-BuLi, followed by quenching with DMF.32 With aldehyde **2a** in hand, we prepared the pyridylbromide coupling partner **4** by reductive amination of **2a** with the *N*-pyridylmethylglycine ethyl ester **3**, which is available in one step from commercially available materials and can be isolated easily by distillation on a multi-gram scale.33 Although the reaction sequence used to prepare **4** proceeded with moderate yields of less than a gram, we observed that isolated yields of **2a** and **4** diminished by roughly 30% for each step upon scale up. We therefore devised an optimized route to the pyridylbromide **4** from **1**, which is compared to the previous method in Scheme 1. In this procedure we prepared alcohol **2b** by reduction of **2a** with $NaBH_4$ *in situ*.32 Isolated yields for **2b** ranged between 54–60% starting with 10 g of **1**. In addition to the higher yield, **2b** could be readily purified by crystallization, in contrast to the aldehyde **2a**, which was difficult to separate from undesired byproducts. Mesylation of **2b** with MsCl and Et_3N afforded a mesylate that was allowed to react with **3** in the presence of K_2CO_3 to furnish **4** in 87% yield over two steps. Using this optimized route, we were able to prepare multi-gram quantities of **4** from **1** in a three step synthetic sequence that required only a single alumina column chromatography purification procedure.

With sufficient amounts of the pyridylbromide **4** in hand, we were able to synthesize large quantities of Et_2BPG_2DEV (**5**) via a cross-coupling reaction between **4** and 4,5-diethynylveratrole (DEV)31 using 10 mol% of $[Pd(PPh_3)_4]$ catalyst in a mixture of Et_3N and THF at 60°C (Scheme 2). We chose the DEV over the DET backbone due to its greater solubility in organic solvents and more facile synthesis. The Sonogashira cross-coupling reaction worked remarkably well upon scale up and the conversion to the reaction product was greater than 90% as determined by ^1H NMR spectroscopy. In order to remove residual

phosphine impurities that were present after purification of the crude product by alumina column chromatography, the HCl salt of the amine was isolated by treatment of an EtOAc solution of the purified material with an etheral hydrogen chloride solution. This purification sequence lowered the isolated yield of the corresponding dihydrochloride salt to 57%. Saponification of the esters with KOH in H_2O proceeded cleanly, affording H_2BPG_2DEV in nearly quantitative yield. Although the salt of the ester is stable for months under ambient atmospheric conditions, the dicarboxylic acid decays to form a complex mixture of products over time as evidenced by ^1H NMR spectroscopy. Therefore, we stored the ligand as the hydrochloride salt of the diester and prepared the acid freshly for the following metal complexation studies.

Synthesis of the Oxo-Bridged Diiron(III) Compounds $[Fe_2(\mu\text{-}O)(H_2O)BPG_2DEV](ClO_4)_2$ (6), $[Fe_2(\mu\text{-}O)(\mu\text{-}O_2CAr^{iPrO})BPG_2DEV](ClO_4)$ (7), $[Fe_2(\mu\text{-}O)(\mu\text{-}CO_3)BPG_2DEV]$ (8)

Compound **6** crystallizes in good yield as deep red-colored blocks by vapor diffusion of Et_2O into a reaction mixture containing H_2BPG_2DEV and two equiv of $Fe(ClO_4)_3{\cdot}9H_2O$ in CH_3CN/H_2O (10:1). The yields and the crystal quality depended strongly on the ratio of CH_3CN and H_2O. Only a few examples of oxo-bridged diiron(III) compounds with aqua ligands have been reported because H_2O is prone to substitution and tends to form oxo-bridged polyiron(III) complexes.43 When excess base, such as NEt_3, was added under aerobic conditions in the synthesis of **6**, the color changed from deep red to intense green. The resulting complex **8** contained a carbonato- and oxo-bridged diiron(III) center that forms upon reaction with CO_2 from the air. This reaction was complete in less than a few seconds when CO_2 gas was introduced directly into the reaction mixture. With the aforementioned procedure, isolated yields of **8** varied widely. Therefore, an optimized protocol for the synthesis of **8** was developed. This procedure involved treating H_2BPG_2DEV with one equiv of the pre-formed (μ-oxo)diiron(III) complex $(Et_4N)_2[Fe_2(\mu\text{-}O)Cl_6]$ dissolved in CH_3OH/CH_2Cl_2, producing a yellow-brown solution. Addition of excess Ag_2CO_3 resulted in nearly instantaneous formation of a green suspension that was stirred for 45 min, filtered, and subjected to vapor diffusion of Et_2O. Emerald-green needles were isolated in 73% yield after several days and analyzed by X-ray crystallography. Compound **8** belongs to a rather rare group of carbonato-bridged diiron complexes.44–50

As with the synthesis of the carbonate complex **8**, the carboxylato-bridged complex **7** could be prepared in a variety of ways in moderate yields, either in a reaction between the ligand H_2BPG_2DEV and two equivalents of $Fe(ClO_4)_3{\cdot}9H_2O$ in the presence of base and excess HO_2CAr^{iPrO}, or by addition of the carboxylic acid to a CH_3CN solution of **6** in the presence of base. Scheme 3 summarizes the pathways for the synthesis of compounds **6**, **7**, and **8**.

Structural Characterization

An ORTEP diagram of **6** is displayed in Fig. 1 and selected bond lengths and angles are reported in Table S2. Compound **6** is a dication and crystallizes with two perchlorate anions in the asymmetric unit and numerous water molecules in the lattice, one of which bridges the two methoxy groups of the veratrole backbone via hydrogen bonds. A packing diagram (Fig. S1 and Table S3, Supporting Information) reveals strong hydrogen-bonding interactions between the H_2O ligands and carboxylate groups of neighboring molecules as well as stacking of the diethynyl-veratrole units. The two iron atoms are separated by 3.4837(9) Å with an Fe-O-Fe angle of 155.37(16)°. The two H_2O molecules bind in a syn fashion with respect to the diiron vector, similar to stoichiometrically analogous complexes that contain either two unlinked BPG^- or two BPP^- (bis(2-pyridylmethyl)aminopropionate) ligands.51,52 In contrast to these two compounds, the pyridine nitrogen atoms of the BPG^- moieties in **6** are bound syn instead of anti to each other, which is a consequence of the linker. Furthermore, the values for the Fe-Fe distance and the Fe-O-Fe angle in **6** are

significantly smaller in comparison to these two complexes (Table 1). In a similar complex with the ligand 6-HPA, where the two neutral TPA units are linked to one another by an ethylene bridge, the distances between the two iron atoms are even longer than 3.56 Å and the Fe-O-Fe angles close to linear.51–53 The shorter distance and angle in **6** are most likely a consequence of more rigid DEV linker, which draws the iron atoms closer together.

Compounds **7** and **8** have very similar structural parameters. These complexes differ in the chemical nature of the bridging ligand, a carboxylate in the case of **7** and a carbonate ion in **8**. Accordingly, compound **7** is positively charged and **8** is neutral. Both diiron cores are displayed in Fig. 2, and crystallographic information and selected bond distances and angles are summarized in Table S2. The BPG_2DEV^{2-} ligand again stabilizes the dinuclear structures by bridging the diiron centers. The carbonato and carboxylato bridges in **7** and **8** lie approximately in the plane defined by the Fe-O-Fe unit, a feature generally observed in these types of compounds.47,54

For compound **7** there are two crystallographically independent molecules in the asymmetric unit and geometric comparisons are reported for averaged values. In **7**, the Fe-Fe distance is 3.218 Å and the Fe-O-Fe angle 128.5°. Compound **8** contains a (μ-oxo)(μ-carbonato)diiron(III) core in which the two iron atoms are separated by 3.1142(18) Å and related by a pseudo-C_2 axis. The Fe-O-Fe angle is 125.97(15)° and the distance to the bridging oxygen atom is 1.740(3) Å, which is consistent with values for other oxo-bridged diiron(III) complexes.55,56

Despite an extensive literature on diiron complexes having tripodal amine ligands, especially TPA derivatives, little has been reported for more carboxylate-rich systems.24,25 In a CSD search, only three crystal structures with the simple BPG^- ligand bound to iron are listed.57 The first has a structure similar to that of **7**, but with a bridging benzoate.54 No reactivity studies of this compound were reported. The second is a hydroxo-bridged diiron compound58 and the third structure contains two H_2O ligands bound to an oxo-bridged diiron core (vide infra).51 Although we obtained evidence for a hydroxo-bridged BPG_2DEV^{2-} diiron(III) complex by mass spectrometry (vide infra), we were not able to isolate such a species.

Spectroscopic Characterization of 6, 7, and 8

The UV-vis spectrum of **6**, which contains only oxo as a bridging ligand, differs dramatically from those of the oxo/carboxylato- and oxo/carbonato-bridged compounds **7** and **8**. Fig. 3 reveals that **6** has a maximum in its optical absorption spectrum around 490 nm, whereas more bands appear in the spectra of **7** and **8,** which are similar to one another. Despite this spectral similarity, the solubilities of the two latter complexes differ significantly. Compound **7** has excellent solubility in CH_3CN and other organic solvents, presumably owing to the lipophilic carboxylate ligand, but **8** is only appreciably soluble in mixtures of CH_3OH/CH_2Cl_2 or CH_3CN/H_2O.

Zero-field Mössbauer spectra of solid samples of **6**, **7**, and **8** were acquired at 4.2 K and/or 90 K. Table 2 summarizes the derived Mössbauer parameters from these experiments and the spectra are displayed in Fig. 4. The isomer shifts acquired at 90 K lie between $\delta = 0.45$ and 0.47 mm/s and quadrupole splitting parameters between $\Delta E_Q = 1.35$ and 1.59 mm/s for the three compounds. These values are characteristic of 6-coordinate high-spin (μ-oxo)diiron(III) complexes, which generally have quadrupole splitting values of > 1 mm/s.55

Fixation of CO_2 to Form the Carbonato-Bridged Complex 8

Complex **6** reacts with atmospheric CO_2 in organic solvents containing triethylamine to form the carbonato-bridged diiron(III) complex **8**. When this reaction was monitored by UV-vis spectroscopy, rapid and quantitative formation of a species having the spectral properties of **8** was apparent (Fig. 5). Even at low temperatures (−78 °C), the reaction occurred in a few seconds following introduction of excess CO_2 (g). Fixation of CO_2 by hydroxo-bridged diiron(II) complexes has been observed previously,59 but only three examples exist in which oxo-bridged diiron(III) complexes react with CO_2 to form carbonato-bridged species.46,47,60

We propose that **8** forms in stepwise manner via formation of a metal hydroxo species. An analogous mechanism was established for the enzyme carbonic anhydrase, which catalyzes the physiologically essential hydration of CO_2 to form bicarbonate.61,62 Deprotonation of a water ligand in **6** could produce a bridging hydroxo ion, which is a reasonable supposition because a diiron species with this composition is observed in the electrospray mass spectrum of **6** under basic conditions (vide infra) and because base is required to promote the reaction in organic solvents. In a second step, nucleophilic attack of the hydroxo ligand on the carbon atom of CO_2 would form bicarbonate. The latter is readily deprotonated to produce the observed carbonato-bridged diiron(III) complex.

Mass Spectrometry – Stability of the Dinuclear Core

The coordination chemistry of complexes **6**, **7**, and **8** is also reflected in ESI mass spectrometry experiments. Mass spectra of the dinuclear complexes dissolved in neutral solution revealed the parent compounds, but in basic aqueous solutions, several new ion clusters are detected. Chart 3 displays the core structures of the resulting diiron species. Two new prominent peaks at m/z = 839 and 883 correspond to positively charged hydroxo- and carbonato-bridged complexes having the formula $[Fe_2(\mu\text{-}O)(\mu\text{-}OH)(BPG_2DEV)]^+$ and $\{[Fe_2(\mu\text{-}O)(\mu\text{-}CO)(BPG_2DEV)]+H\}^+$ (**8**), respectively. The hydroxo-bridged complex can form either by substitution of a bridging ligand by OH^- or by deprotonation of a ligated H_2O molecule in **6**. Although no crystal structure was obtained that revealed this particular unit, it is reasonable to propose that the core can readily form, by analogy to related diiron(III) complexes with a BPG^- ligand and derivatives thereof.51,58 The carbonato-bridged species most likely derives from a reaction in basic solution of the diiron complex with atmospheric CO_2, as occurs during the synthesis of **8**. Since complex **6** contains labile H_2O ligands, it is not surprising that a peak corresponding to the parent ion is not observed in the mass spectrum. When excess carboxylic or carbamic acid was added to solutions of **6**, **7**, and **8**, a dominant peak for the corresponding carboxylate- or carbamate-bridged species was observed. Interestingly, very bulky carboxylates could also be introduced this manner, suggesting that even sterically hindered bridging ligands are accommodated by the platform (data not shown). In contrast to the described systems, analogous Fe–O–Fe complexes containing non-covalently linked BPG^- units and derivatives thereof readily dissociate or oligomerize to give mononuclear or trinuclear complexes, respectively.51,58

Reaction of 6, 7, and 8 with H_2O_2 – Characterization of a Common Peroxo Intermediate

(a) UV-vis Spectroscopic Studies—When **6**, **7**, and **8** were treated with excess H_2O_2 in the presence of a small amount of NEt_3, the solutions turned to a more intense, maroon color, concomitant with evolution of a gaseous product. A test with an alkaline pyrogallol-solution confirmed the formation of dioxygen.63,64 The intermediate products from reactions with H_2O_2, **6a**, **7a**, and **8a**, in solutions of CH_3CN/H_2O were monitored by UV-vis spectroscopy. Buildup of a broad visible absorption band at 490 nm (ε = 1500 M^{-1} cm^{-1}) was observed in all three cases. The corresponding spectra are presented in Fig. 6 and in

Figs. S5 and S6. When the reactions were repeated without the addition of NEt_3, the solutions turned yellow and no spectra analogous to those for **6a**, **7a**, or **8a** were observed. The formation rate of **6a**, **7a**, and **8a** was strongly dependent on the amount of H_2O_2 used. An excess of ca. 1000 equiv of H_2O_2 was required to achieve the maximum absorption intensity at 490 nm for the carbonato-bridged complex **8** over a period of more than an hour. With compound **7**, which has a bridging carboxylate ligand, the band maximized more rapidly (ca. 10–15 min) in the presence of a smaller amount of H_2O_2 (ca. 50–100 equiv, Fig. S5). In contrast, only 5–10 equiv of H_2O_2 and less than a minute of reaction time were required to form **6a** (Fig. S6). These observations are consistent with loss of a H_2O ligand occurring more readily than the less labile monoanionic carboxylate or dianionic carbonate ligands. Intermediates **6a**, **7a**, and **8a** were also observed in other solvent mixtures, including CH_3OH/H_2O and CH_2Cl_2/CH_3OH. When **6a** was generated in a solution of aqueous methanol, an absorption with essentially the same features as found for **6a** in CH_3CN/H_2O was observed, but the peak maximum shifted from 490 nm to 470 nm (Fig. S7).

Reaction of **8** with 1000-fold excess H_2O_2 and a catalytic amount of base was monitored by UV-vis spectroscopy, as displayed in Fig. 6. Early in the time course of the reaction (ca. 90 min), the intermediate builds up but it subsequently decays to a species having a similar absorption spectrum as the starting material. After a second addition of a 1000-fold excess of H_2O_2, the band at 490 nm reappears. These experiments, together with mass spectral evidence, reveal that the oxo-bridged diiron core remains largely intact and is most likely bridged by a carbonate ligand because of the similarity of the final spectrum to that of the starting material.

(b) Mössbauer Spectroscopic Studies—Zero-field Mössbauer spectra of frozen solution samples of **6a**, **7a**, and **8a** were acquired at 90 K. The spectrum of **6a** is shown in Fig. 7, and those for **7a** and **8a** are displayed in Figs. S8 and S9. Mössbauer parameters for the three compounds are listed in Table 3. A sample of **8a** (in CH_3CN/H_2O) was measured at 4.2 K and fit to two quadrupole doublets with an area ratio of 78:22. Because of limited solubility, the sample contains nearly 80% of starting material **8**, which can be assigned to one of the doublets. The second doublet, however, belongs to the reaction intermediate **8a** with an isomer shift of $\delta = 0.63(6)$ mm/s and quadrupole splitting parameter of $\Delta E_Q = 0.64(6)$ mm/s. Similarly, in the 90 K spectrum of **7a** (in CH_3OH/H_2O), there is evidence for a population of the starting material **7** in the spectrum, together with another quadrupole doublet assigned to a species having $\delta = 0.58(2)$ mm/s and $\Delta E_Q = 0.56(2)$ mm/s. The best conversion to the intermediate was achieved in a reaction of a dilute (ca. 2 mM) solution of ^{57}Fe-enriched **6** with H_2O_2 and base. Here, 66% of **6a** was generated with Mössbauer parameters of $\delta = 0.58(2)$ mm/s and $\Delta E_Q = 0.58(2)$ mm/s, identical within error limits to those for **7a**. Taking into account that the spectrum of **8a** was acquired at temperatures and from solvents different than those of **6a** and **7a**, the data strongly suggest that **6a**, **7a**, and **8a** are the same species. The presence of a single quadrupole doublet is most consistent with two high-spin iron sites symmetrically bridged by a peroxo-ligand.

We were interested to learn whether the starting diiron complex reforms upon completion of reactions with H_2O_2, as implied by the UV-vis spectroscopic experiments. We therefore measured a frozen solution sample [CH_3OH/H_2O (20:1)] of the decomposition product from a reaction of **6** with ca. 50 equiv of H_2O_2 and a trace of NEt_3. The Mössbauer parameters of $\delta = 0.46(3)$ mm/s and $\Delta E_Q = 1.39(3)$ mm/s were very similar to those for the starting material **6** ($\delta = 0.45(3)$ mm/s; $\Delta E_Q = 1.51(3)$ mm/s) in the same basic solution mixture. We conclude that this species is most likely a (μ-oxo)(μ-hydroxo)diiron(III) complex and that no decomposition occurred (vide supra and Chart 3).

The spectroscopic and mass spectrometric (vide infra) data determined for the common intermediate formed in the H_2O_2 reactions of **6**, **7**, and **8** are characteristic of a (μ-oxo)(μ-peroxo)diiron(III) complex. Table 4 lists some examples of transient peroxo species observed in pre-steady-state studies of non-heme diiron enzymes and of oxo-bridged diiron(III) model systems. Well-defined peroxodiiron(III) intermediates are observed in sMMOH, RNR-R2, and Δ^9D^4 and in the T201S variant of ToMOH20 that display characteristic peroxo ligand-to-metal charge transfer (LMCT) bands between 650 to 750 nm and Mössbauer parameters of $\delta = 0.62–0.68$ mm/s and $\Delta E_Q > 1.0$ mm/s.4 In contrast, the recently characterized, putative peroxodiiron(III) intermediate of ToMOH has Mössbauer isomer shifts smaller than $\delta = 0.6$ mm/s, quadrupole splitting parameters significantly less than 1 mm/s ($\Delta E_Q = 0.66$ mm/s), and lack an optical band in their absorption spectra.65 These significant differences can be rationalized by a different peroxo coordination mode and/or protonation state. Synthetically prepared peroxodiiron(III) complexes have the peroxo ligand generally bound in a μ-1,2-fashion with spectroscopic properties very similar to those of peroxo intermediates in the former group of enzymes.5 The UV-vis and Mössbauer spectroscopic properties of the peroxodiiron(III) intermediate reported here, however, differ significantly from these complexes. To our knowledge, of all the synthetic examples of (μ-oxo)(μ-peroxo)diiron(III) species, only the intermediates reported here, **6a**, **7a**, and **8a**, have a Mössbauer quadrupole splitting parameter that is nearly identical to the values for colorless peroxo intermediates in ToMOH and PHH. In addition to their unique Mössbauer spectroscopic properties, intermediates **6a**, **7a**, and **8a** display a considerably blue-shifted LMCT band, assigned by RR spectroscopy (see below), in their UV-vis spectra compared to other peroxodiiron(III) species (Table 4). A comparison with two (μ-oxo)(μ-peroxo)diiron(III) complexes providing an N_4 (6-Me_3-TPA)66 and a closely related N_3O (6-Me_2-BPP) coordination environment on each iron atom,67 similar to that supplied by the BPG^- unit, display LMCT bands at 648 nm and 577 nm, respectively, consistent with the carboxylate being a stronger donor. This observation might explain the hypsochromic shift in intermediates containing the BPG_2DEV^{2-} ligand.

(c) EPR Spectroscopy—EPR spectroscopic analysis of **8a** reveals an axial signal with g values of 2.062 and 2.004, which we attribute to a mixed-valent diiron(II,III) ($S = ½$) species. Spin quantitation indicated only 2.6% abundance, however. The bulk of the sample is EPR-silent, which we assign to two iron(III) centers antiferromagnetically coupled to one another. This result is consistent with a peroxo-bridged diiron(III) complex.5 The absence of an EPR signal centered at $g = 4.3$, characteristic for mononuclear high-spin iron(III) complexes, is also in agreement with these findings. The EPR spectrum is displayed as Fig. S12.

(d) Resonance Raman Spectroscopy—RR spectra of intermediate **6a**, prepared with either $H_2\,^{16}O_2$ (or $H_2\,^{18}O_2$) and obtained with 568-nm excitation, revealed two features at 819 and 845 (772 and 797) cm^{-1}, respectively (Fig. 8). These RR signals are not observed in samples that were allowed to proceed in time beyond decay of intermediate **6a** (Fig. 8B). The intensities of the RR doublets also decrease after prolonged laser exposure and photobleaching of the samples from dark brown to light yellow. Relative to solvent bands, these intensities also vary with excitation wavelength, revealing a significant decrease at 647 nm and at 413 nm, where intra-pyridine vibrations enter into resonance (Fig. 9). Because of the complexity of these RR signals and the photosensitivity of intermediate **6a**, extracting excitation profiles would be an overinterpretation of the data. Nevertheless, the excitation wavelength dependence of the isotope-sensitive signals qualitatively matches expectation based on the absorption spectra of intermediate **6a** (Fig. S6).

The observed RR frequencies and ^{18}O-shifts (−47/−48 cm^{-1}) are consistent with metal-peroxo vibrations. The ν(O–O) frequencies in symmetrically-bridged (μ-1,2-peroxo)diiron(III) complexes range from 830 to 908 cm^{-1} and low frequency O–O stretching bands are generally correlated with short Fe-Fe distances.69–71 The RR bands associated with ν(O–O) in intermediate **6a** are at the lower end of this range and a comparison to these systems indicates that the Fe-Fe distance in intermediate **6a** may be as short as 3.1–3.2 Å. Short Fe-Fe distances require stabilization from bridging ligands in addition to the peroxo group, with a μ-oxo group providing the shortest such distance. Although Fe-O-Fe modes were not identified in the RR spectra of intermediate **6a**, it is reasonable to assume that the oxo bridge, present in the starting material, remains in intermediate **6a**. This assignment is strongly supported by mass spectrometric analysis (vide infra). The covalent linkage between the two iron sites supplied by the syn *N*-donor ligand BPG$_2$DEV^{2-} may also play an important role in promoting a short Fe-Fe distance. In a similar peroxodiiron(III) species, with a dinucleating ligand having two covalently linked tris(2-pyridyl)methane moieties, the O–O mode of the bound peroxide appears at very low value of 830 cm^{-1}, which is consistent with this hypothesis.71,72

From spectroscopic studies we can conclude that the peroxo ligand bridges the two iron centers in **6a**, but we cannot definitively assign its binding mode. Detailed experimental and theoretical studies on (μ-oxo)(μ-1,2-peroxo)diiron(III) intermediates having unlinked tetradentate capping ligands, related to those in BPG$_2$DEV^{2-}, confirmed the 1,2-peroxo bridging mode. Furthermore, a crystal structure of [Fe$_2$(μ-O)(μ-1,2-O$_2$)6-Me$_2$-BPP] (see Table 4), which has an identical ligand set to that of **6a**, reveals a 1,2-bridging peroxo ligand lying approximately in the plane defined by the Fe-O-Fe unit.67 The spectroscopic properties and the O–O stretching frequencies of the peroxodiiron(III) compound described here, however, differ significantly from those reported for these species and we cannot rule out an alternative peroxo binding mode. Because the mass spectra of **6a–8a** reveal the presence of an added proton as well as the peroxo ligand (vide infra), the structure might contain a μ-1,1-hydroperoxodiiron(III) unit in which the dangling O-atom is protonated, a unit that is consistent with all of the data.

The presence of a doublet rather than a single peak for the isotope-sensitive RR bands may result either from two different conformations of the peroxodiiron complex or Fermi splitting of a fundamental O–O stretch corresponding to the doublet average of 832 cm^{-1}. Fermi coupling of the ν(O–O) with underlying non-resonant vibrations has been invoked for several peroxodiiron complexes.10,17,66,70 On the other hand, the possible occurrence of two distinct peroxodiiron species must also be taken into consideration, perhaps reflecting different protonation states. Optical spectroscopic73 and kinetic studies indicate the presence of two peroxo intermediates in the oxygenation chemistry of sMMOH and ToMOH.20 In the low-frequency region, the [^{16}O-intermediate – ^{18}O-intermediate] RR difference spectrum isolates a positive feature at 479 cm^{-1} that may correspond to the expected ν(Fe-^{16}O$_2$) mode, even though its negative ^{18}O-counterpart does not emerge from the broad and nearly featureless background signal that occurs in this region (Fig. 8).

(e) Mass Spectrometry—ESI-MS of **6a**, **7a**, and **8a** were acquired using solutions of CH$_3$CN/H$_2$O (3:1) or CH$_2$Cl$_2$/CH$_3$OH (1:1) in low- and high-resolution modes. In each high-resolution mass spectrum of **6a**, **7a**, and **8a** there was an ion cluster having a mass and isotope pattern identical to that calculated for the M+H (peroxo)diiron(III) species {[Fe$_2$(μ-O)(μ-O$_2$)BPG$_2$DEV]+H}$^+$ with a theoretical *m/z* = 855.1195. The recorded values were *m/z* = 855.1205, 855.1189, and 855.1161 for **6a**, **7a**, and **8a**, respectively. A comparison between the theoretical and observed spectra is presented in Fig. S13. Isotope-labeling experiments carried out with H$_2^{18}_2$O$_2$ (2% in H$_2$O) revealed a peak shift of four units from *m/z* = 855 to

859, demonstrating that the peroxide is bound to the diiron center. A comparison of the two mass spectra is shown in Fig. 10.

Singly-charged ion clusters of $[Fe_2(\mu\text{-}O)(\mu\text{-}OH)(BPG_2DEV)]^+$ (*m/z* = 839) and $\{[Fe_2(\mu\text{-}O)(\mu\text{-}CO_3)(BPG_2DEV)]+H\}^+$ (*m/z* = 883) were also observed in these mass spectra, which derive from the reaction of the diiron complex with hydroxide and CO_2 from the air (vide supra). Interestingly, two additional peaks at *m/z* = 841 and 885 were detected in the ^{18}O-labeled sample. These values are shifted by two mass units from the peaks for these two diiron complexes, indicating that an ^{18}O atom is incorporated into the hydroxo- and carbonato-bridged compounds, respectively. This result suggests that the O–O bond of the bound peroxide is indeed cleaved and, presumably, that H_2O is formed. An O–O bond scission is reasonable, because this reaction has been investigated extensively in related (μ-oxo)(μ-1,2-peroxo)diiron(III) complexes, which form high-valent diiron centers, and has been proposed for a similar compound in a dinucleating ligand system.25,53,74 The intermediate could react with another equivalent of H_2O_2 to form H_2O and O_2. We propose that the newly formed H_2O molecule stays bound to the diiron center and can readily be deprotonated under basic conditions to form a bridging hydroxide ion. Such an intermediate could additionally react with CO_2 from air to form the carbonato-bridged species. By mass spectrometry, we were able to establish that the peroxo species is regenerated upon additional treatment with H_2O_2 (data not shown).

Catalase Activity

When H_2O_2 was added to a basic solution of the diiron compounds **6**, **7**, or **8**, O_2 formation was observed, as confirmed by a test with an alkaline pyrogallol solution.63,64 The catalase-like activity of the carbonato complex **8** was investigated in more detail and the O_2 formed in the reactions was quantified. To a fixed concentration of diiron(III) complex **8** and NEt_3 in a solution of CH_3CN/H_2O (2:1) at 0 °C were added various amounts of H_2O_2. The quantity of O_2 produced was measured volumetrically. The yield of O_2 depends linearly on the amount of H_2O_2, with a slope of 0.53 (R^2 = 0.99), which corresponds to catalase-like reaction stoichiometry (Fig. 11 and eq. 1). The diiron catalyst is very efficient and achieves ~10,000 turnovers. Experiments

$$2H_2O_2 \rightarrow O_2+2H_2O \quad (1)$$

with compounds **6** and **7** under the same conditions revealed them to be as efficient as **8** with respect to catalase function.

Catalase activity has been reported in reactions of a relatively small number of oxo-bridged diiron(III) compounds with H O 75–80 In all cases, intermediates with spectroscopic properties characteristic for peroxo-bridged diiron(III) complexes were observed. Some common features of these H_2O_2-disproportionation catalysts include complex decomposition, TON (turn-over number) dependence on the exchangeability of the bridging ligand, and increasing O_2 formation rates at higher pH values. In contrast, to these previously reported systems, decomposition of the complexes **6**, **7**, and **8** upon treatment with H_2O_2 does not occur. The increased stability of the complexes is attributed to the BPG_2DEV^{2-} ligand. Remarkably, quantitative O_2 production is observed for all three complexes **6**–**8**, with TONs significantly higher than those reported for other systems (the ratio of $[Fe_2]$:H_2O_2 never exceeded 1:500) and only when base was added to the reaction mixture. In samples that were lacking additional base, quantitative O_2 production was not observed.

Catalase activity is important for protecting the cell from oxidative damage by excess H_2O_2. A ubiquitous family of metalloenzymes disproportionate H_2O_2 in an exothermic reaction to

form H_2O and dioxygen. One of the two most abundant classes of catalases contains an iron protoporphyrin IX cofactor with an axial tyrosinate ligand.81 The second most common catalase enzyme contains a dimanganese active site.82 For non-heme diiron enzymes, catalase activity has been reported for ToMOH83 and toluene-2-monooxygenase from *Burkholderia cepacia* G4,84. By comparison with previous studies of diiron model compounds, the present findings are important for our general understanding of catalase activity in BMMs and the decomposition pathway of H_2O_2 catalyzed by diiron centers.

Substrate Oxidation

We also investigated whether the peroxo intermediates **6a**, **7a**, and **8a** might function as oxidases. The common intermediate quantitatively oxidizes PPh_3 to Ph_3PO, a very easy conversion, but is a poor catalyst for the epoxidation of *cis*-cyclooctene, unlike some related systems.53,85,86 Quantitation of the epoxide revealed yields < 1% and TONs of ca. 8 and 3, for **6a** and **7a**, respectively (Table S4). The production of O_2 was strongly diminished by addition of phosphine to the reaction, but was not significantly affected when cyclooctene was present, which is consistent with competitive catalase and substrate oxidation reactions.

Summary and Perspective

This study describes the successful application of the dinucleating ligand H_2BPG_2DEV to specifically model the syn coordination of histidine residues in non-heme diiron enzymes. This scaffold is more biologically relevant than previous versions due to its greater carboxylate content. Three (μ-oxo)diiron(III) derivatives were characterized, one with a terminal water molecule on each iron atom and two with additional bridging ligands, either carbonate or carboxylate. Reactivity studies with H_2O_2 show that the dinucleating ligand conveys an inherent stability to all three oxo-bridged diiron complexes, which serve as catalases in multi-turnover reactions with large excesses of H_2O_2. These characteristics distinguish these complexes from the broader class of diiron(III) complexes that do not have covalently linked tripodal ligands. The present system belongs to a small group of non-heme diiron model complexes having catalase activity that dominates over its oxygenating properties. Similar catalase activity has been observed in ToMOH and PHH, suggesting additional relevance of the present model complexes to biological counterparts. Spectroscopic analysis of a transient (μ-oxo)(μ-peroxo)diiron(III) species generated in this chemistry reveals properties that deviate from the characteristic parameters for peroxo-bridged intermediates in most model complexes and non-heme diiron enzymes. The Mössbauer spectroscopic properties closely resemble those for a peroxo intermediate in ToMOH, with ΔE_Q values less than 1 mm/s. Raman studies reveal an O–O stretching frequency that is atypically low, suggesting a short iron-iron distance in the peroxo intermediate, presumably facilitated by the dinucleating ligand and possibly reflecting a previously unknown μ-1,1 bridging mode. These physical properties of these complexes differentiate them from compounds with mononucleating ligands. Further studies of related complexes are warranted in pursuit of information to understand the origin of the spectroscopic properties and reactivity of non-heme diiron sites in biology.

Supplementary Material

Refer to Web version on PubMed Central for supplementary material.

Acknowledgments

This work was supported by grants GM032134 (SJL) and GM74785 (PM-L) from the National Institute of General Medical Sciences. We thank Ms. Wanhua Ye at the Chemistry Department at Tufts University and Ms. Li Li at the

DCIF at MIT for help with mass spectrometric measurements, Dr. Sebastian Stoian for assistance in acquiring the EPR spectra, and Drs. Peter Müller and Daniela Buccella for assistance with X-ray crystallography.

References

(1). Feig AL, Lippard SJ. Chem. Rev. 1994; 94:759–805.

(2). Wallar BJ, Lipscomb JD. Chem. Rev. 1996; 96:2625–2657. [PubMed: 11848839]

(3). Kurtz DM Jr. J. Biol. Inorg. Chem. 1997; 2:159–167.

(4). Merkx M, Kopp DA, Sazinsky MH, Blazyk JL, Müller J, Lippard SJ. Angew. Chem., Int. Ed. 2001; 40:2782–2807.

(5). Solomon EI, Brunold TC, Davis MI, Kemsley JN, Lee S-K, Lehnert N, Neese F, Skulan AJ, Yang Y-S, Zhou J. Chem. Rev. 2000; 100:235–349. [PubMed: 11749238]

(6). Sturgeon BE, Burdi D, Chen S, Huynh B-H, Edmondson DE, Stubbe J, Hoffman BM. J. Am. Chem. Soc. 1996; 118:7551–7557.

(7). Logan DT, Su XD, Åberg A, Regnström K, Hajdu J, Eklund H, Nordlund P. Structure. 1996; 4:1053–1064. [PubMed: 8805591]

(8). Bollinger JM Jr. Edmondson DE, Huynh BH, Filley J, Norton JR, Stubbe J. Science. 1991; 253:292–298. [PubMed: 1650033]

(9). Lindqvist Y, Huang W, Schneider G, Shanklin J. EMBO J. 1996; 15:4081–4092. [PubMed: 8861937]

(10). Broadwater JA, Ai J, Loehr TM, Sanders-Loehr J, Fox BG. Biochemistry. 1998; 37:14664–14671. [PubMed: 9778341]

(11). Sazinsky MH, Lippard SJ. Acc. Chem. Res. 2006; 39:558–566. [PubMed: 16906752]

(12). Murray LJ, Lippard SJ. Acc. Chem. Res. 2007; 40:466–474. [PubMed: 17518435]

(13). Cafaro V, Izzo V, Scognamiglio R, Notomista E, Capasso P, Casbarra A, Pucci P, Di Donato A. Appl. Environ. Microbiol. 2004; 70:2211–2219. [PubMed: 15066815]

(14). Sazinsky MH, Bard J, Di Donato A, Lippard SJ. J. Biol. Chem. 2004; 279:30600–30610. [PubMed: 15096510]

(15). Sazinsky MH, Dunten PW, McCormick MS, DiDonato A, Lippard SJ. Biochemistry. 2006; 45:15392–15404. [PubMed: 17176061]

(16). Kuzelka J, Farrell JR, Lippard SJ. Inorg. Chem. 2003; 42:8652–8662. [PubMed: 14686842]

(17). Moënne-Loccoz P, Baldwin J, Ley BA, Loehr TM, Bollinger JM. Biochemistry. 1998; 37:14659–14663. [PubMed: 9778340]

(18). Rinaldo D, Philipp DM, Lippard SJ, Friesner RA. J. Am. Chem. Soc. 2007; 129:3135–3147. [PubMed: 17326634]

(19). Lee S-K, Lipscomb JD. Biochemistry. 1999; 38:4423–4432. [PubMed: 10194363]

(20). Song WJ, Behan RK, Naik SG, Huynh BH, Lippard SJ. J. Am. Chem. Soc. 2009; 131:6074–6075. [PubMed: 19354250]

(21). Lee S-K, Fox BG, Froland WA, Lipscomb JD, Münck E. J. Am. Chem. Soc. 1993; 115:6450–6451.

(22). Liu KE, Valentine AM, Wang D, Huynh BH, Edmondson DE, Salifoglou A, Lippard SJ. J. Am Chem. Soc. 1995; 117:10174–10185.

(23). Du Bois J, Mizoguchi TJ, Lippard SJ. Coord. Chem. Rev. 2000; 200-202:443–485.

(24). Tshuva EY, Lippard SJ. Chem. Rev. 2004; 104:987–1012. [PubMed: 14871147]

(25). Que L Jr. Tolman WB. Angew. Chem., Int. Ed. 2002; 41:1114–1137.

(26). Tolman WB, Que L Jr. J. Chem. Soc., Dalton Trans. 2002; 5:653–660.

(27). Baik M-H, Gherman BF, Friesner RA, Lippard SJ. J. Am Chem. Soc. 2002; 124:14608–14615. [PubMed: 12465971]

(28). Kodanko Jeremy J, Morys Anna J, Lippard Stephen J. Org. Lett. 2005; 7:4585–4588. [PubMed: 16209485]

(29). Kodanko JJ, Xu D, Song DT, Lippard SJ. J. Am. Chem. Soc. 2005; 127:16004–16005. [PubMed: 16287269]

(30). Kodanko JJ, Lippard SJ. Inorg. Chim. Acta. 2008; 361:894–900.
(31). Reisner E, Lippard SJ. Eur. J. Org. Chem. 2008; 2008:156–163.
(32). Wang X, Rabbat P, O'Shea P, Tillyer R, Grabowski EJJ, Reider PJ. Tetrahedron Lett. 2000; 41:4335–4338.
(33). Policar C, Lambert F, Cesario M, Morgenstern-Badarau I. Eur. J. Inorg. Chem. 1999:2201–2207.
(34). Armstrong WH, Lippard SJ. Inorg. Chem. 1985; 24:981–982.
(35). Dunbar KR, Longridge JJ, Rawson JM, Sun J-S, Hagen KS, Do B. Inorg. Synth. 2002; 33:103–107.
(36). Gumanov LL, Shteinman AA, Nordlander E, Koldobskii GI. Russ. J. Org. Chem. 2002; 38:606–608.
(37). SMART, Software for the CCD Detector System. version 5.6. Bruker AXS; Madison, WI: 2000.
(38). Sheldrick, GM. SHELXTL-97. University of Göttingen; Göttingen, Germany: 2000.
(39). Sheldrick GM. Acta Crystallogr., Sect. A. 2008; A64:112–122. [PubMed: 18156677]
(40). Sheldrick, GM. SADABS: Area-Detector Absorption Correction. University of Göttingen; Göttingen, Germany: 2001.
(41). Spek, AL. PLATON, A Multipurpose Crystallographic Tool. Utrecht University; Utrecht, The Netherlands: 2000.
(42). Kent, TA. WMOSS. Minneapolis: 1998.
(43). Lippard SJ. Angew. Chem., Int. Ed. 1988; 27:344–361.
(44). Schmitt W, Hill JP, Malik S, Volkert CA, Ichinose I, Anson CE, Powell AK. Angew. Chem., Int. Ed. 2005; 44:7048–7053.
(45). Schmitt W, Hill JP, Juanico MP, Caneschi A, Costantino F, Anson CE, Powell AK. Angew. Chem., Int. Ed. 2005; 44:4187–4192.
(46). Glaser T, Lügger T, Hoffmann R-D. Eur. J. Inorg. Chem. 2004:2356–2362.
(47). Hazell R, Jensen KB, McKenzie CJ, Toftlund H. J. Chem. Soc., Dalton Trans. 1995:707–717.
(48). Fujita T, Ohba S, Nishida Y, Goto A, Kokii T. Acta Crystallogr., Sect. C. 1994; C50:544–546.
(49). Arulsamy N, Hodgson DJ, Glerup J. Inorg. Chim. Acta. 1993; 209:61–69.
(50). Norman RE, Holz RC, Menage S, Que L Jr. Zhang JH, O'Connor CJ. Inorg. Chem. 1990; 29:4629–4637.
(51). Mortensen MN, Jensen B, Hazell A, Bond AD, McKenzie CJ. J. Chem. Soc., Dalton Trans. 2004:3396–3402.
(52). Hazell A, Jensen KB, McKenzie CJ, Toftlund H. J. Chem. Soc., Dalton Trans. 1993:3249–3257.
(53). Kodera M, Itoh M, Kano K, Funabiki T, Reglier M. Angew. Chem., Int. Ed. 2005; 44:7104–7106.
(54). Menage S, Que L Jr. New J. Chem. 1991; 15:431–438.
(55). Kurtz DM Jr. Chem. Rev. 1990; 90:585–606.
(56). Drüeke S, Wieghardt K, Nuber B, Weiss J. Inorg. Chem. 1989; 28:1414–1417.
(57). ConQuest. Cambridge Crystallographic Data Center; 2007.
(58). Furutachi H, Ohyama Y, Tsuchiya Y, Hashimoto K, Fujinami S, Uehara A, Suzuki M, Maeda Y. Chem. Lett. 2000:1132–1133.
(59). Kitajima N, Hikichi S, Tanaka M, Morooka Y. J. Am. Chem. Soc. 1993; 115:5496–5508.
(60). Schmitt W, Anson CE, Sessoli R, van Veen M, Powell AK. J. Inorg. Biochem. 2002; 91:173–189. [PubMed: 12121774]
(61). Silverman DN, Lindskog S. Acc. Chem. Res. 1988; 21:30–36.
(62). Vahrenkamp H. Acc. Chem. Res. 1999; 32:589–596.
(63). Duncan IA, Harriman A, Porter G. Anal. Chem. 1979; 51:2206–2208.
(64). Williams DD, Blachly CH, Miller RR. Anal. Chem. 1952; 24:1819–21.
(65). Murray LJ, García-Serres R, Naik S, Huynh BH, Lippard SJ. J. Am. Chem. Soc. 2006; 128:7458–7459. [PubMed: 16756297]
(66). Dong Y, Zang Y, Shu L, Wilkinson EC, Que L Jr. Kauffmann K, Münck E. J. Am. Chem. Soc. 1997; 119:12683–12684.

(67). Zhang X, Furutachi H, Fujinami S, Nagatomo S, Maeda Y, Watanabe Y, Kitagawa T, Suzuki M. J. Am. Chem. Soc. 2005; 127:826–827. [PubMed: 15656607]

(68). Kodera M, Taniike Y, Itoh M, Tanahashi Y, Shimakoshi H, Kano K, Hirota S, Iijima S, Ohba M, Okawa H. Inorg. Chem. 2001; 40:4821–4822. [PubMed: 11531426]

(69). Brunold TC, Tamura N, Kitajima N, Moro-oka Y, Solomon EI. J. Am. Chem. Soc. 1998; 120:5674–5690.

(70). Moënne-Loccoz P, Krebs C, Herlihy K, Edmondson DE, Theil EC, Huynh BH, Loehr TM. Biochemistry. 1999; 38:5290–5295. [PubMed: 10220314]

(71). Fiedler AT, Shan X, Mehn MP, Kaizer J, Torelli S, Frisch JR, Kodera M, Que L Jr. J. Phys. Chem. A. 2008; 112:13037–13044. and references therein. [PubMed: 18811130]

(72). Kodera M, Itoh M, Kano K, Funabiki T. Bull. Chem. Soc. Jpn. 2006; 79:252–261.

(73). Brazeau BJ, Lipscomb JD. Biochemistry. 2000; 39:13503–13515. [PubMed: 11063587]

(74). Xue G, Fiedler AT, Martinho M, Münck E, Que L Jr. Proc. Natl. Acad. Sci. U.S.A. 2008; 105:20615–20620.

(75). Mauerer B, Crane J, Schuler J, Wieghardt K, Nuber B. Angew. Chem., Int. Ed. 1993; 32:289–291.

(76). Balogh-Hergovich E, Speier G, Reglier M, Giorgi M, Kuzmann E, Vertes A. Eur. J. Inorg. Chem. 2003:1735–1740.

(77). Than R, Schrodt A, Westerheide L, Van Eldik R, Krebs B. Eur. J. Inorg. Chem. 1999:1537–1543.

(78). Ito S, Okuno T, Matsushima H, Tokii T, Nishida Y. J. Chem. Soc., Dalton Trans. 1996:4479–4484.

(79). Okuno T, Ito S, Ohba S, Nishida Y. J. Chem. Soc., Dalton Trans. 1997:3547–3551.

(80). Menage S, Vincent JM, Lambeaux C, Fontecave M. J. Chem. Soc., Dalton Trans. 1994:2081–2084.

(81). Maté MJ, Murshudov G, Bravo J, Melik-Adamyan W, Loewen PC, Fita I. Handb. Metalloproteins. 2001; 1:486–502.

(82). Wu AJ, Penner-Hahn JE, Pecoraro VL. Chem. Rev. 2004; 104:903–938. [PubMed: 14871145]

(83). Murray LJ, Naik SG, Ortillo DO, GarcíaSerres R, Lee JK, Huynh BH, Lippard SJ. J. Am. Chem. Soc. 2007; 129:14500–14510. [PubMed: 17967027]

(84). Newman LM, Wackett LP. Biochemistry. 1995; 34:14066–76. [PubMed: 7578004]

(85). White MC, Doyle AG, Jacobsen EN. J. Am. Chem. Soc. 2001; 123:7194–7195. [PubMed: 11459514]

(86). Taktak S, Kryatov SV, Haas TE, Rybak-Akimova EV. J. Mol. Catal. A: Chem. 2006; 259:24–34.

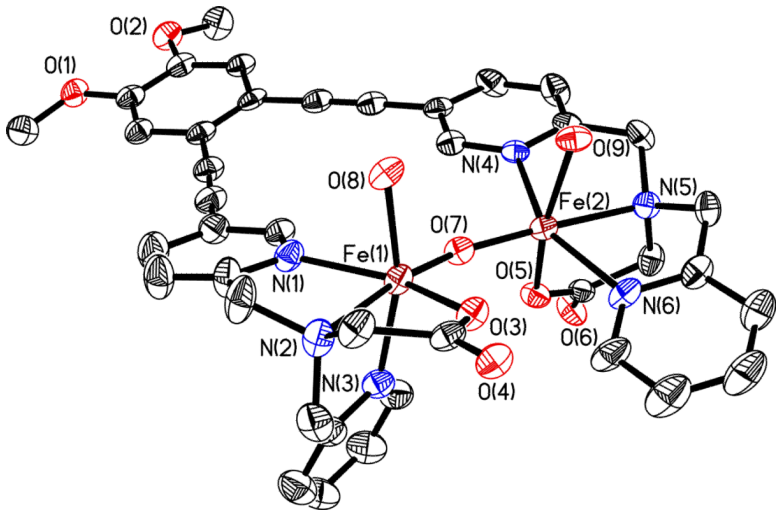

Figure 1.
ORTEP diagram of **6** displaying thermal ellipsoids (40%). For clarity, the ClO_4^- anions are not shown.

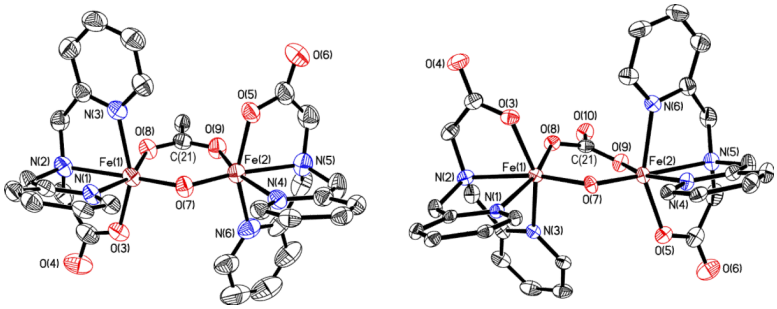

Figure 2.

ORTEP diagram of **7** (left) and **8** (right) displaying thermal ellipsoids (50%). For clarity, the diethynylveratrole backbones, the Ar$^{i\text{Pr}}$O group, and the ClO_4^- anion are not shown.

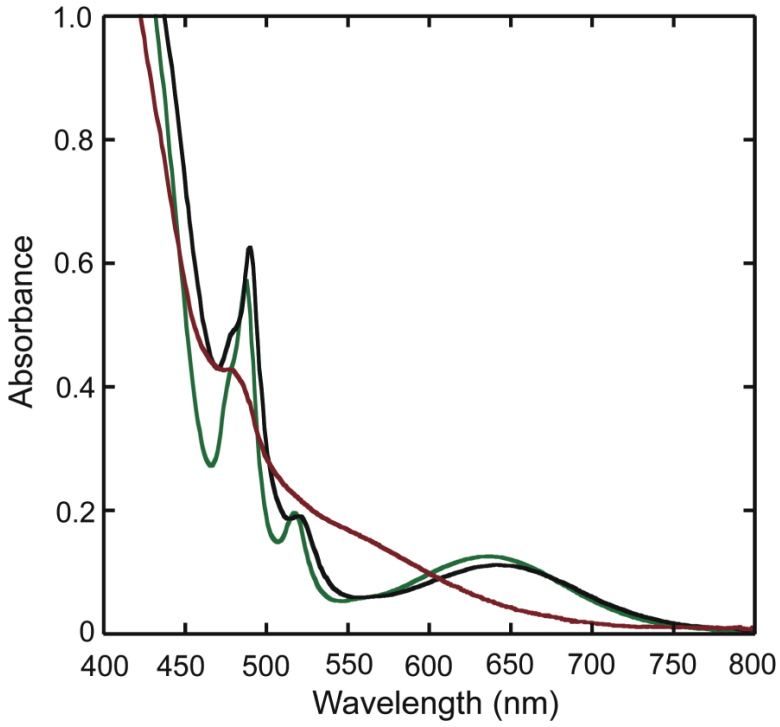

Figure 3.
UV-vis absorption spectra of 1 mM solutions of **7** (black) and **8** (green) in $CH_3OH/CHCl_3$ (1:1) and of **6** (red) in CH_3CN/H_2O (10:1).

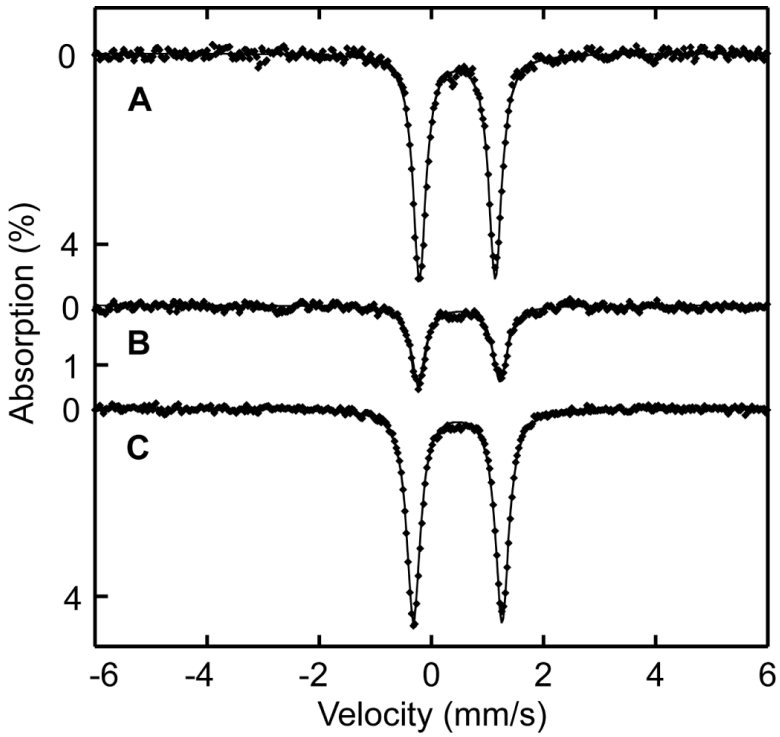

Figure 4.
Zero-field Mössbauer spectrum of **8** (A), **7** (B), and **6** (C) acquired at 90 K [experimental data (❶) and calculated fits (—)].

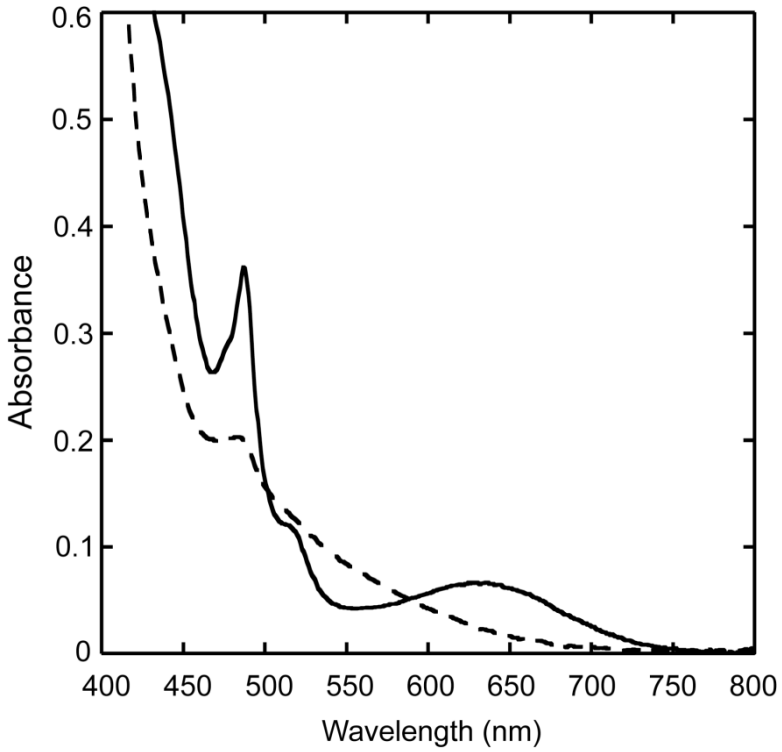

Figure 5.
UV-vis spectra of **6** before (- - -) and after reaction with CO_2 (—) in a basic CH_3OH/CH_2Cl_2 (1:1) solution.

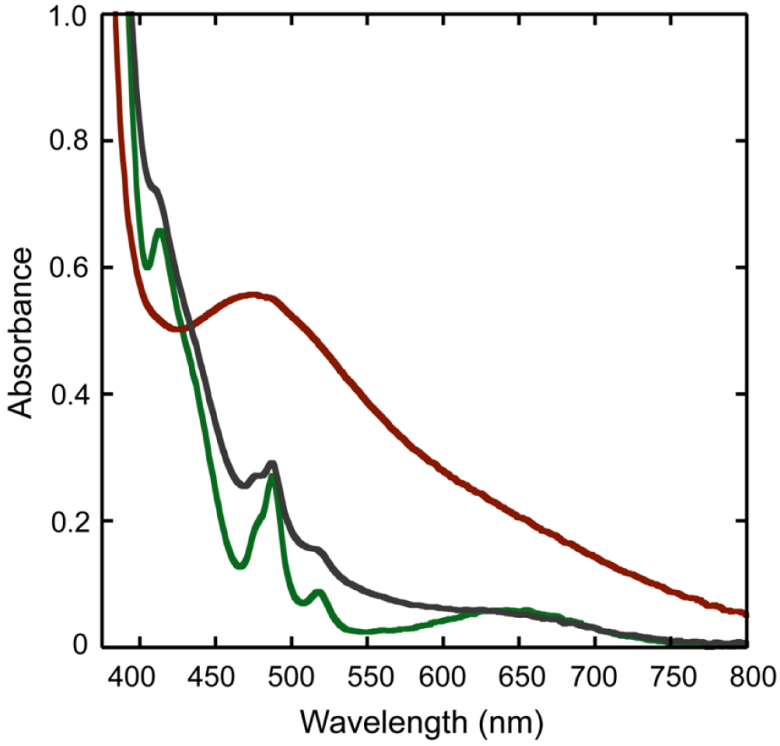

Figure 6.

UV-vis spectra, recorded at 0 °C, of a reaction mixture of **8** (0.37 mM, green trace) in CH_3CN/H_2O (2:1), NEt_3, and H_2O_2 to form a peroxo intermediate **8a** (red trace). The grey trace corresponds to the product from the reaction.

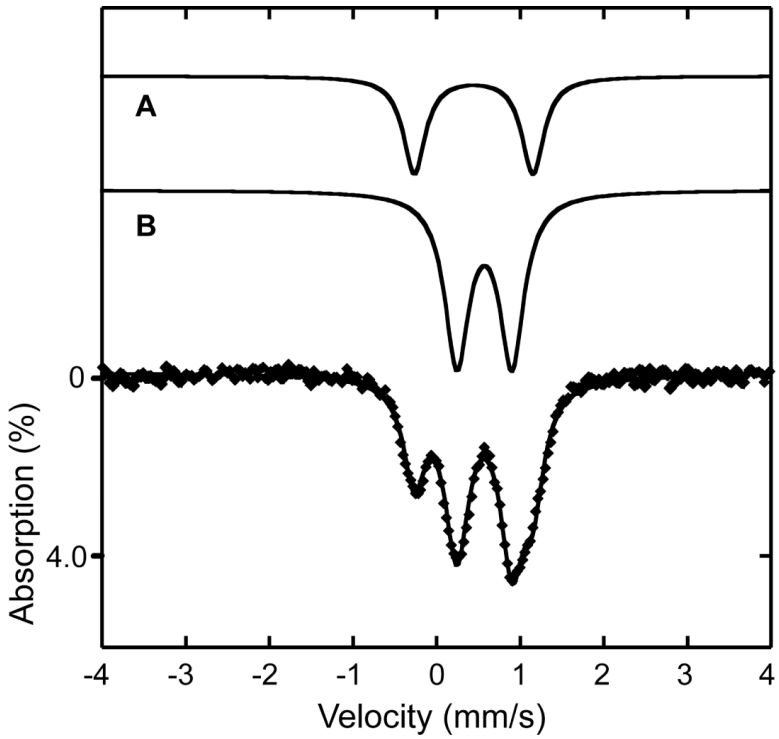

Figure 7.

Zero-field Mössbauer spectrum [experimental data (❶) and calculated fits (—)] recorded at 90 K for a frozen solution sample of the product of the reaction of **6** with excess H_2O_2 and a trace of NEt_3. The sample contained 66% of **6a** (B) and 34% of a diiron(III) species (A; δ = 0.45 mm/s and ΔE_Q = 1.41 mm/s) with Mössbauer parameters similar to those of the starting material.

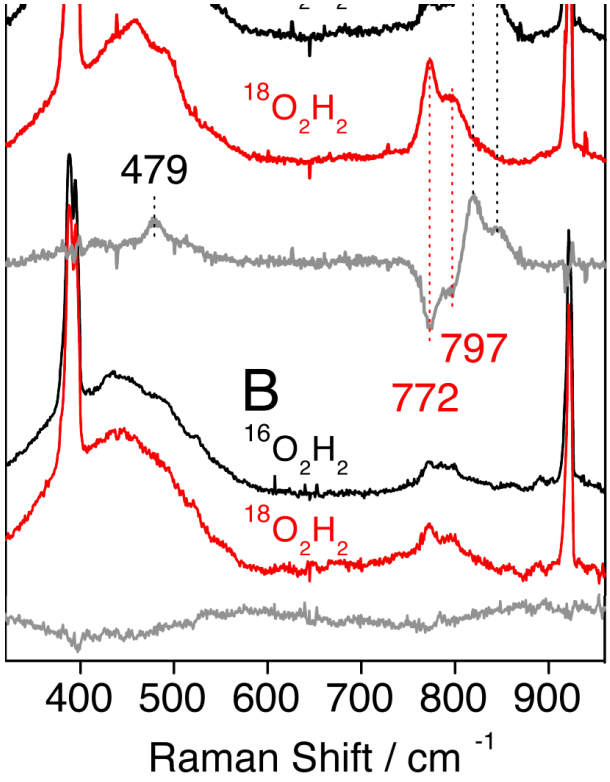

Fig. 8.

RR spectra of intermediate **6a** (A) and its decomposition product (B) obtained with 568-nm excitation at 110 K. Sharp Raman bands below 400 and above 900 cm^{-1} correspond to solvent vibrations.

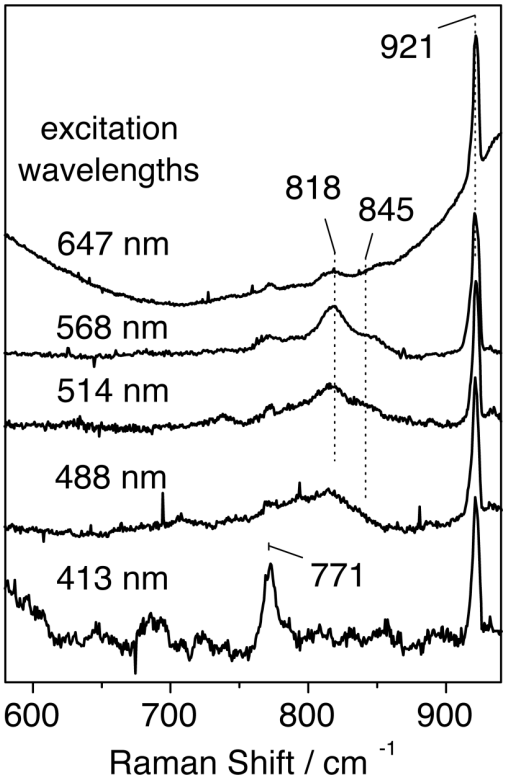

Fig. 9.
RR spectra of intermediate **6a** obtained with different laser excitations at 110 K. All traces are normalized to the 921-cm^{-1} solvent band.

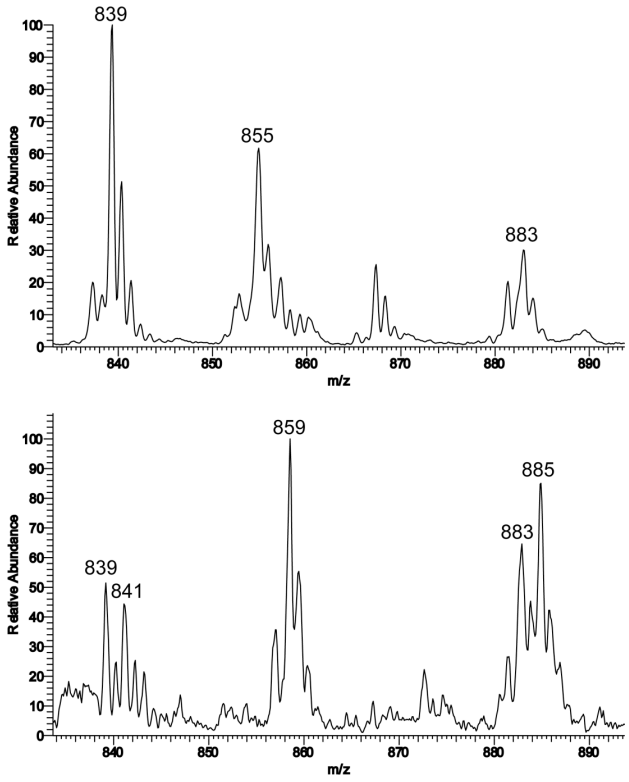

Figure 10.

ESI mass spectrum of **7a** at 295 K in CH_3CN displaying the isotope patterns for ions at *m/z* = 855 for {[Fe_2(μ-O)(μ-$^{16}O_2$)BPG_2 DEV]+H^+} (top) and *m/z* = 859 for for {[Fe_2(μ-O)(μ-$^{18}O_2$)BPG_{22} DEV]+H^+} (bottom). The peak *m/z* = 867 in the upper spectrum can be assigned to a formate-bridged diiron complex [Fe_2(μ-O)(μ-O CH)BPG_2DEV]$^+$, which is due to the presence of residual formic acid impurities.

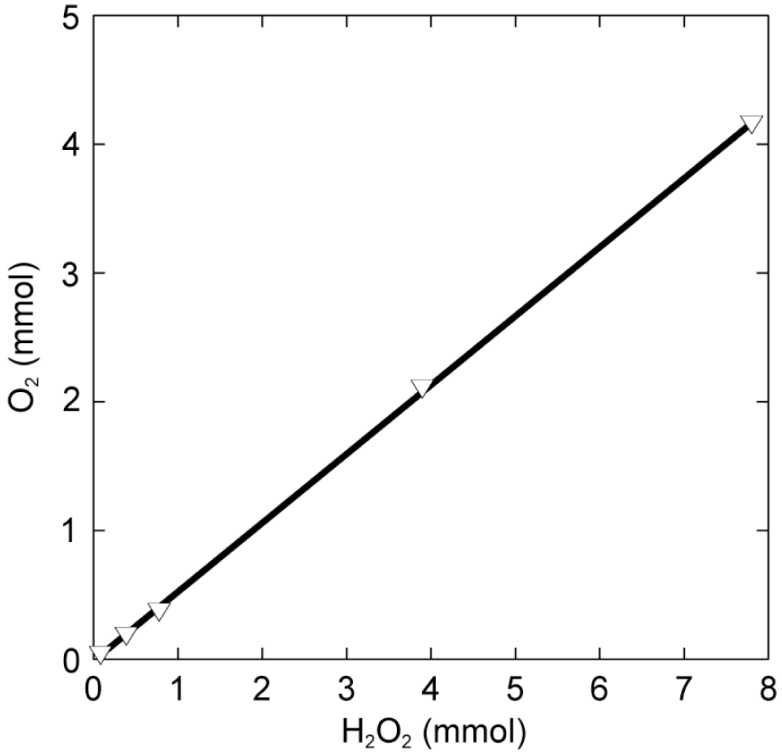

Figure 11.

O_2 formation from 0.078 to 7.8 mmol H_2O_2 at 0 °C as catalyzed by **8** (2 mL of 0.4 mM solution in CH_3CN/H_2O, 2:1) and 10 μL of NEt_3.

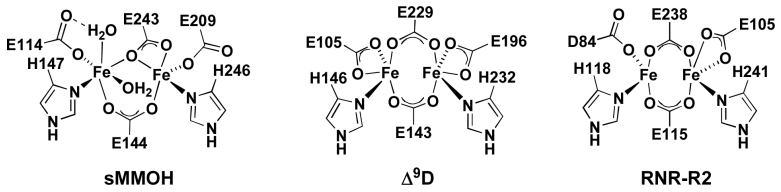

Chart 1.

$Ar^{Tol}CO_2^-$, R = CH_3
$Ar^{4\text{-}FPh}CO_2^-$, R = F
$Ar^{Mes}CO_2^-$, R' = R = CH_3

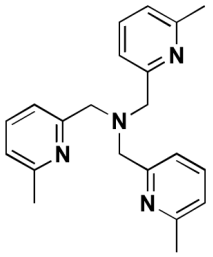

6-Me_3-TPA

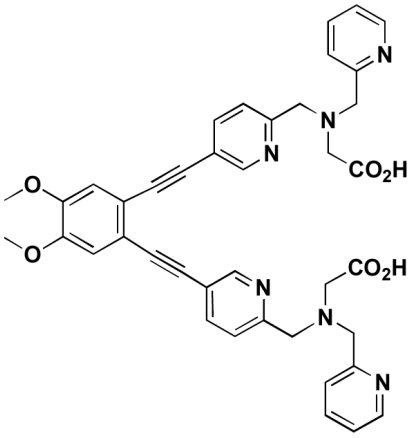

H_2BPG_2DEV

Chart 2.

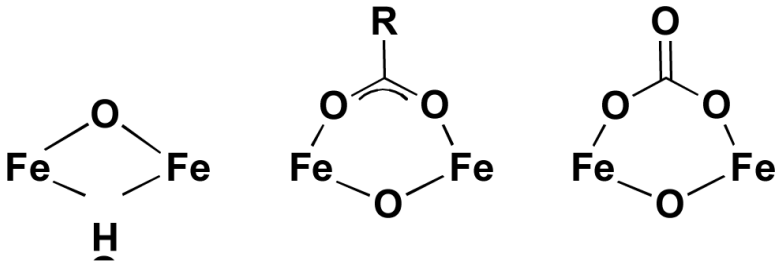

Chart 3.

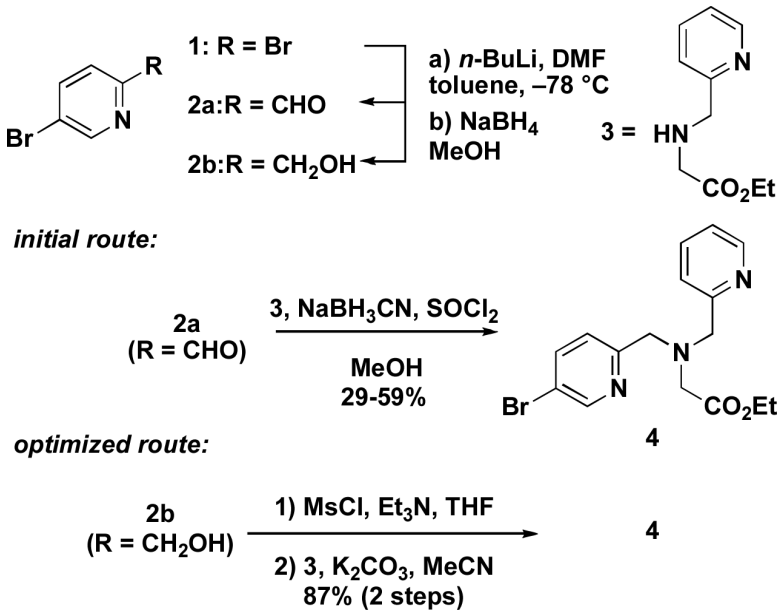

Scheme 1.
Preparation of pyridylbromide **4**.

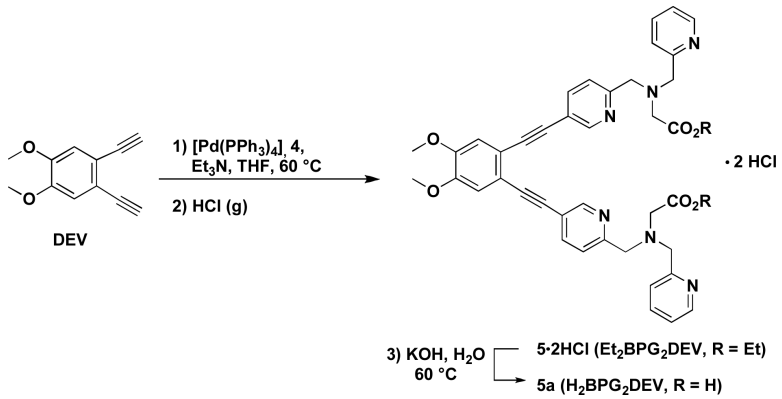

Scheme 2.

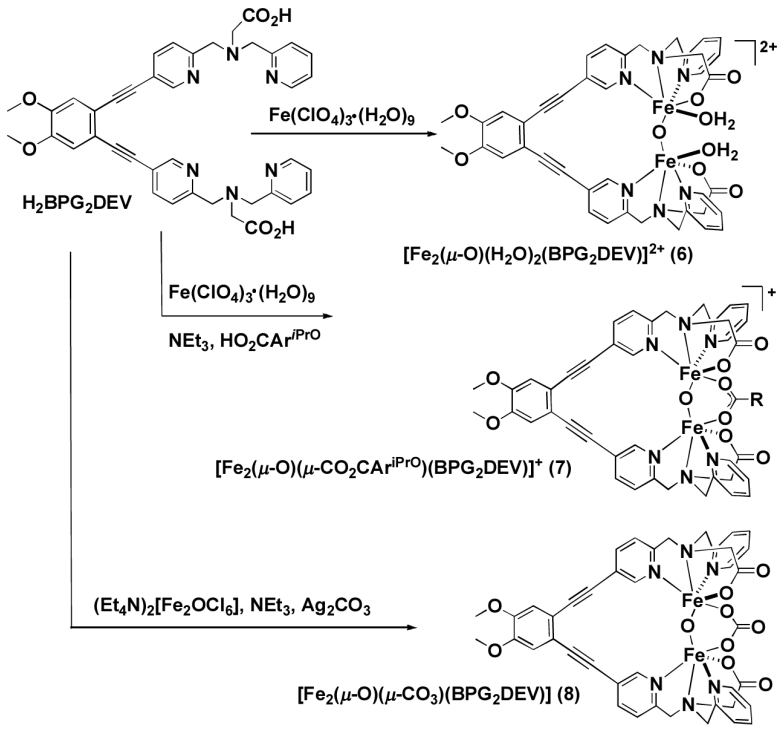

Scheme 3.

Table 1

Comparison of Fe-Fe Distances and Fe-O-Fe Angles (deg) of Diiron Compounds with a $[Fe_2(\mu\text{-}O)(H_2O)_2]$ Core.

Compound	Fe-Fe (Å)	Fe-O-Fe (deg)	Ref.
6	3.4837(9)	155.37(16)	*a*
$[Fe_2(\mu\text{-}O)(H_2O)_2BPG_2]^{2+}$	3.56	169.8(2)	51
$[Fe_2(\mu\text{-}O)(H_2O)_2BPP_2]^{2+}$	3.564(2)	168.8(3)	52
$[Fe_2(\mu\text{-}O)(H_2O)_2(6\text{-}HPA)_2]^{4+}$	3.607(3)	179.2	53

Abbreviations: BPP = bis(2-pyridylmethyl)aminopropionate; 6-HPA = 1,2-bis[2-{bis(2-pyridylmethyl)aminomethyl}-6-pyridyl]ethane.

[a]This work.

Table 2

Zero-Field Mössbauer Parameters of Solid **6**, **7**, and **8**, Acquired at 90 K.

Compound	δ (mm/s)	ΔE_Q (mm/s)	Γ (mm/s)
6	0.47(2)	1.59(2)	0.29
7	0.46(2)	1.47(2)	0.31
8	0.47(2)[a]	1.35(2)[a]	0.28[a]
	0.45(2)	1.36(2)	0.31

[a]Acquired at 4.2 K.

Table 3

Zero-Field Mössbauer Parameters of Intermediates **6a**, **7a**, and **8a**, Acquired at 90 K.

	δ (mm/s)	ΔE_Q (mm/s)	Γ (mm/s)
6a	0.58(2)	0.58(2)	0.35
7a	0.58(2)	0.56(2)	0.29
8a	0.63(6)	0.64(6)	0.32

Table 4

Spectroscopic Parameters for Peroxo Intermediates in Non-Heme Diiron Enzymes and Synthetic Oxo-Bridged Diiron(III) Compounds.

	Optical		Mössbauer		
	γ_{max} (nm)	ε ($M^{-1}cm^{-1}$)	δ (mm/s)	ΔE_Q (mm/s)	Ref.
sMMOH (*M. caps.* (Bath))	700	1800	0.66	1.51	*a*
ToMOH (*Pseudomonas* sp. OX1)	-	-	0.54	0.66	65
ToMOH T201S (*Pseudomonas* sp. OX1)	675	1500	0.67	1.51	20
RNR-R2 D84E	700	1500	0.63	1.58	*a*
Δ^9-desaturase	700	1200	0.68	1.90	*a*
$[Fe_2(\mu\text{-}O)(\mu\text{-}1,2\text{-}O_2)(6\text{-}Me_3\text{-}TPA)_2]^{2+}$	494; 648[c]	1100; 1200	0.54	1.68	66
$[Fe_2(\mu\text{-}O)(\mu\text{-}1.2\text{-}O_2)(\mu\text{-}O_2CR)(hexpy)_2]^{+}$	510; 605[c]	1300; 1310	0.53	1.67	68
$[Fe_2(\mu\text{-}O)(\mu\text{-}1,2\text{-}O_2)(6\text{-}Me_2\text{-}BPP)_2]$	577	1500	0.50	1.46	67
$[Fe_2(\mu\text{-}O)(\mu\text{-}O_2)BPG_2DEV]$	490	1500	0.58	0.58	*b*

[a] Parameters were taken from ref. 1.

[b] This work.

[c] peroxo-Fe(III) charge transfer band.